SIAM J. Applied Dynamical Systems
Vol. 22, No. 4, pp. 3165–3207

Centrality-Based Traffic Restriction in Delayed Epidemic Networks*

Atefe Darabi† and Milad Siami†

Abstract. In an epidemic network, lags due to travel time between populations, latent period, and recovery period can significantly change the epidemic behavior and result in successive echoing waves of the spread between various population clusters. Moreover, external shocks to a given population can propagate to other populations within the network, potentially snowballing into waves of resurgent epidemics. The main objective of this study is to investigate the effect of time delay and small shocks/uncertainties on the linear susceptible-infectious-susceptible (SIS) dynamics of epidemic networks. In this regard, the asymptotic stability of this class of networks is first studied, and then its performance loss due to small shocks/uncertainties is evaluated based on the notion of the $\mathcal{H}_2$ norm. It is shown that network performance loss is correlated with the structure of the underlying graph, intrinsic time delays, epidemic characteristics, and external shocks. This performance measure is then used to develop an optimal traffic restriction algorithm for network performance enhancement, resulting in reduced infection in the metapopulation. A novel epidemic-based centrality index is also defined to evaluate the impact of every subpopulation on network performance, and its asymptotic behavior is investigated. It is shown that for specific choices of parameters, the output of the epidemic-based centrality index converges to the results obtained by local or eigenvector centralities. Moreover, given that epidemic-based centrality depends on the epidemic properties of the disease, it may yield distinct node rankings as the disease characteristics slowly change over time or as different types of infections spread. This node interlacing phenomenon is not observed in other centralities that rely solely on network structure. This unique characteristic of epidemic-based centrality enables it to adjust to various epidemic features. The derived centrality index is then adopted to improve the network robustness against external shocks on the epidemic network. The numerical results, along with the theoretical expectations, highlight the role of time delay as well as small shocks in investigating the most effective methods of epidemic containment.

Key words. delayed networks, infection waves, centrality measures, dynamical systems, optimizations, traffic restrictions

MSC codes. 93C95, 93B35, 93B60, 15B51, 05C90, 05C50

DOI. 10.1137/22M1507760

1. Introduction.

The large-scale spread of an infectious disease is a recurring phenomenon may potentiallylead to severe crises before the disease eventually dies out or turns into an endemic [53]. The extent to which a highly contagious disease continues propagating depends

*Received by the editors July 28, 2022; accepted for publication (in revised form) by I. Belykh August 18, 2023; published electronically November 28, 2023. The views and conclusions contained in this document are those of the authors and should not be interpreted as necessarily representing the official policies, either expressed or implied, of the U.S. Department of Homeland Security.

https://doi.org/10.1137/22M1507760

Funding: This material is based upon work supported by the U.S. Department of Homeland Security under grant 22STESE00001-01-00. This research was also supported in part by NSF grants 2208182 and 2121121 and by ONR grant N00014-21-1-2431.

†Department of Electrical and Computer Engineering, Northeastern University, Boston, MA 02115 USA (darabi.a@northeastern.edu, m.siami@northeastern.edu).

on several factors, such as intervention policies and the existence of an effective treatment. The study of epidemic propagation by network models has shown great potential in designing effective epidemic management methods as well as allocating treatment and immunization resources [71, 74].

The macro-modeling (or metapopulation) representation of epidemic diseases is widely studied in the literature [3, 5, 66]. Several studies have incorporated compartmental networked models such as susceptible-infected-susceptible (SIS) [12, 32, 48, 65], Susceptible-infected-removed (SIR) [36, 62], susceptible-infected-quarantined-susceptible (SIQS) [33], and susceptible-exposed-asymptomatic-infectious-recovered (SEAIR) [31] to capture the epidemic behavior at community levels. In many studies, the effect of internal time delays resulting from the latent period of a disease has been included by considering an extra compartment called *exposed,* e.g., susceptible-exposed-infected-removed (SEIR) model [34, 36, 39]. However, given that an infinite-dimensional system of delayed differential equations (DDEs) is not representable by a set of ordinary differential equations (ODEs) with a finite dimension, the behavior of models with an exposed compartment is not necessarily identical to models that directly include the effect of internal time delays [28, 72]. Consequently, epidemic models defined based on ODEs (with or without considering the exposed group) fail to show the successive waves of epidemic, common in several epidemic diseases [4, 47], unless time-varying epidemic rates are incorporated [2, 41]. Various models such as delayed SIR model [77], forced-SIR-based (FSIR) model [30], SIR model with adjustable parameters [42], SEIR-based model [61], and SIR-based model [11] have been employed to estimate the fluctuations in infection progress. Unlike models that include a removed compartment, the SIS model allows for the possibility of an endemic disease, which means that the disease persists in the population at a low level over time. Therefore, it is considered a more appropriate model for studying the impact of interventions. This situation is more realistic for many infectious diseases, especially those that do not provide long-lasting immunity after infection or vaccination. This study is based on the SIS model to gain clear insight into the effect of the proposed traffic restriction policies on the epidemic's progress.

Network stability is another aspect of dynamic epidemic networks that requires special attention when designing disease mitigation policies. The stability of linear networks with time delay is widely studied in the literature [25, 26, 38, 40, 70]. More specifically for epidemic studies, the stability of networked SIS models without time delay has been extensively investigated in the literature [17, 20, 35, 37, 58]. Regarding the delayed systems, an exact numerical approach for determining the regions of stability for delayed linear systems is proposed in [45]. The stability of linear networks with single or multiple delays has been studied in [14, 44, 52]. We use the provided results in those references to acquire the delay-dependent range of stability for the class of networks studied in this paper.

In addition to stability, a delayed network's robustness against external noises may be dependent on internal delays as well, which makes it necessary to further investigate the role of time delays on the network performance. From the network robustness point of view, the performance of noisy linear consensus networks has been investigated in [59], where a performance measure based on the $\mathcal{H}_2$ norm of the system is introduced and established for networks with different types of input noise. The proposed performance measure is then adopted to analyze the robustness of delayed networks with linear SIS dynamics against exogenous noises

[13]. The $\mathcal{H}_2$ norm of delayed linear time-invariant (LTI) systems has also been developed by solving the delay Lyapunov equation, where a spectral discretization scheme is offered for systems with commensurate and noncommensurate time delays [27]. The effect of microscopic shocks on the robustness of economic networks has been studied, where component-level disruptions can potentially lead to macroscopic outcomes [1, 55, 56]. In our study, the effect of small shocks, which might stem from unpredictable minor changes in the transportation network, for instance, is considered and the performance of certain epidemic networks subject to those disruptions is investigated to analyze the influence of network structure and epidemic characteristics on the network robustness.

Identification of influential individuals within a network strongly depends on the centrality measures used, which vary based on the specific application and the criteria under consideration. Some studies have investigated the correlation between various centralities that are defined based on network structure (adjacency matrix) [64]. For instance, it is shown that parameterized centralities like Katz centrality and subgraph centrality can be "tuned" to interpolate between walk-based centralities such as degree and eigenvector centrality [9]. It is also shown that diffusion centrality [7] is proportional to other prominent indices like degree, eigenvector, or Katz centrality for certain choices of parameters [8]. In an epidemic network, in addition to network structure, the characteristics of epidemic disease will affect the role of nodes, which makes it necessary to introduce customized centralities tailored to epidemic mitigation problems. There is a great body of research on epidemic elimination and disease spread control [21, 57, 75, 76], where various methods such as node/edge removal [48, 49, 63, 67] or intercity traffic restriction [50] are applied. However, to the best of our knowledge, the employment of centralities based on epidemic properties has received less attention, which motivated us to introduce a novel epidemic-based centrality to rank the network nodes based on their location and the status of epidemic disease.

Our contributions. This study is dedicated to the epidemiological investigation of infectious diseases with the following main contributions:

i. Although the effect of latent period can be captured by introducing the *exposed* compartment to a model, we believe that time delay is an intrinsic property of epidemic networks, capable of transforming their behavior in a unique manner. For instance, to the best of our knowledge, the oscillatory behavior in the infection progress does not appear when employing an SEIS model [15, 69]. While the SEIS model has been extensively studied, there has been limited research on the impact of time delay on epidemic networks. In this regard, we first present the SIS dynamics of epidemic networks affected by time delay. The objective is to investigate the role of network properties and time delays in emerging successive epidemic waves under linear SIS dynamics (section 2).

ii. We then evaluate the stability and robustness of such delayed systems against external shocks affecting the epidemic network. A metric of network performance is employed to analyze performance sensitivity against noises and delays (section 3).

iii. A specific epidemic-based node centrality index is then defined to evaluate the role of each node in epidemic progress when an exogenous noise is present. Unlike many widely used centralities, e.g., degree or eigenvector centrality, this epidemic-based centrality measure does not merely depend on network structure; it is affected by epidemi-

ological properties of the disease, such as epidemic rates and internal time delays. This unique characteristic makes the proposed centrality index an ideal candidate for identifying the key nodes in epidemic networks. The relationship between epidemic-based centrality and some well-known centralities is also found. Because our epidemic-based centrality is dependent on epidemic properties of the disease, for a given transportation network (with a fixed structure) the epidemic-based centrality will result in different rankings for different diseases. Therefore, in such cases, different node rankings, i.e., interlacing nodes, are expected when employing epidemic-based centrality. On the other hand, when an infection remains in the network for a sufficiently long time, its characteristics may change in a quasi-static manner. This phenomenon can also result in having interlacing nodes in the network. It is, therefore, crucial to identify interlacing nodes and modify traffic restriction measures accordingly to enable effective mitigation of the epidemic (section 4).

iv. The proposed performance measure is next utilized to develop a traffic restriction algorithm to prevent the epidemic network from losing performance while reducing average infection among its nodes. Furthermore, a second optimization framework is developed to investigate the effect of noise distribution on network performance and provide a robust traffic restriction approach for the worst cases (section 5).

The simulation results for a core-periphery network and also for the network of busiest U.S. airports are presented in section 6. It is worth mentioning that because the main purpose of this study is to gain insight into the role of delays in epidemic progress by providing analytical results, a simple 2-compartmental model like SIS is a suitable candidate for avoiding unnecessary complications.

2. Delayed SIS model for epidemic networks.

2.1. Preliminaries and definitions.

Mathematical notation. Let $\mathcal{G} = (\mathcal{V}, \mathcal{E}, w)$ represent an undirected and weighted graph, where $\mathcal{V} = \{1, 2, \ldots, n\}$ for $n \in \mathbb{N}$ shows the set of nodes in the graph. $\mathcal{E} \subset \mathcal{V} \times \mathcal{V}$ denotes the edge set, which provides the map of connection between pairs of nodes in $\mathcal{V}$ with the corresponding weight of $w(e) = w_e \in \mathbb{R}_+$ for all $e = \{i, j\} \in \mathcal{E}$, where $\mathbb{R}_+$ is the set of nonnegative real numbers. $\mathbf{w} \in \mathbb{R}^m$ is the vector of edge weights defined as $\mathbf{w} = [w_1, w_2, \ldots, w_m]$, where $m = |\mathcal{E}|$. Note that $|.|$ denotes the cardinality of a set. The adjacency matrix of the corresponding network is then defined by $A = [a_{ij}] \in \mathbb{R}^{n \times n}$, where $a_{ij} = w(e)$ if $e = \{i, j\} \in \mathcal{E}$. The diagonal elements of A are defined next.

Epidemic network description. In the following subsections, we consider an epidemic network comprising n subpopulations/nodes in $\mathcal{V}$, where each subpopulation can be in one of two states, susceptible to the infectious disease or infected by the disease. The map of connection between the subpopulations is given by set $\mathcal{E}$. The interpopulation connection strength, i.e., traffic flow, is denoted by $0 < a_{ij} = w_e \leq 1$ for all $e \in \mathcal{E}$. The disease progress in each subpopulation of the network depends on its intrapopulation and interpopulation connections as well as epidemic rates of the disease. While the effect of interpopulation connections is reflected through the off-diagonal elements of the adjacency matrix, its diagonal elements indicate the intensity of intrapopulation contacts. We project the final effect of local social distancing between members of subpopulation i on a_{ii}, where $a_{ii} \to 0$ belongs to a

subpopulation following the local social distancing, and $a_{ii} \to 1$ indicates that the local social distancing rules become less strict.

2.2. Stochastic and deterministic SIS metapopulation model with time delay. In this subsection, we introduce the stochastic SIS model of a delayed epidemic network with underlying graph $\mathcal{G}$ and use the mean-field theory to develop the deterministic delayed SIS model. Two sources of time delay are considered in this study: the time it takes for a susceptible individual to become infectious, and the time required to recover from the disease. For simplicity, we assume that both time delays have the same value and that all subpopulations/nodes experience the same time delay, denoted by τ. The mean-field theory has been widely utilized to develop the nondelayed SIS model [18, 19, 43, 68], and we use the results in [18, 66] to develop the delayed version of the SIS model by mean-field approximation.

Let us consider a node i in the network $\mathcal{G}$. At time t, node i can be in one of two states: susceptible or infected. We represent the state of node i at time t using a binary random variable, denoted by $x_i(t)$, which takes the value 1 if node i is infected and 0 if it is susceptible. As time evolves, the state of each node i changes according to a stochastic process parameterized by epidemic properties of the disease and the internal time delay. The probability of an infected individual infecting others while in contact with them, also known as the infection rate of a disease, is denoted by $\beta \in \mathbb{R}_+$, and the probability of recovering from the disease, also known as the recovery rate of a disease, is denoted by $\delta \in \mathbb{R}_+$.

If node i is susceptible at time t, it can become infected during the time interval $(t, t+\Delta t]$ with a probability that depends on the infection rate, the strength of node i's connections to its infected in-neighbors, denoted by a_{ij} for $j \in \mathcal{N}_i$, and the state of its in-neighbor nodes at time $t-\tau$, denoted by $x_j(t-\tau)$ for $j \in \mathcal{N}_i$. We can express the probability of node i transitioning from a susceptible state to an infected state by

$$\Pr\left(x_i(t+\Delta t) = 1 \mid x_i(t) = 0, \mathbf{x}(t-\tau)\right) \approx \sum_{j=1}^{n} \beta a_{ij} x_j(t-\tau)\Delta t. \tag{2.1}$$

This approximation is valid when the infection rate is small. If node i is infected at time $t-\tau$, its probability of recovering is dependent on the recovery rate δ. The probability of i transitioning to a susceptible state during $(t, t+\Delta t]$ is

$$\Pr\left(x_i(t+\Delta t) = 0 \mid x_i(t-\tau) = 1, x_i(t) = 1, \mathbf{x}(t-\tau)\right) \approx \delta \Delta t. \tag{2.2}$$

The state of an epidemic network consisting of n nodes is determined by all the possible combinations of states in which the nodes can be at any given time. As a result, the size of the state space increases exponentially as the network size grows, making the networked SIS epidemic model difficult to analyze. To avoid this computational complexity, we apply the mean-field theory to the described Markov chain and approximate it using a system of differential equations.

Let the random variable $q_i(t) = 1_{\{x_i(t)=1\}}$ be defined such that $q_i(t) = 1$ when node i is infected and 0 otherwise. Therefore, $q_i(t)$ changes according to the state $x_i(t)$ of node i at each time step, which itself depends on the status of i and its neighbors τ time steps before. If node i is susceptible at t and has been in contact with its infected in-neighbors during

$[t-\tau, t-\tau+\Delta t]$, it transitions to an infected state with rate $\sum_{j=1}^{n} \beta a_{ij} x_j(t-\tau)\Delta t$ during $(t, t+\Delta t]$. If node i is infected at $t-\tau$, it will recover with rate $\delta\Delta t$ during $(t, t+\Delta t]$. Using (2.1) and (2.2), we can describe the change of $q_i(t)$ in a sufficiently small time interval Δt as follows:

$$\frac{q_i(t+\Delta t) - q_i(t)}{\Delta t} = \left(1 - 1_{\{x_i(t-\tau)=1\}}\right) \sum_{j=1}^{n} \beta a_{ij} x_j(t-\tau) - 1_{\{x_i(t-\tau)=1\}}\delta. \tag{2.3}$$

Next, we denote the probability of infection at node i as $p_i(t)$. Then, $p_i(t) = \Pr(x_i(t) = 1) = \mathbb{E}[q_i(t)]$, and we have that the probability of infection $p_i(t)$ at node i evolves according to

$$\frac{p_i(t+\Delta t) - p_i(t)}{\Delta t} = \sum_{j=1}^{n} \beta a_{ij} p_j(t-\tau) - \delta p_i(t-\tau) - \mathbb{E}\left[1_{\{x_i(t-\tau)=1\}} \beta \sum_{j=1}^{n} a_{ij} 1_{\{x_j(t-\tau)=1\}}\right]. \tag{2.4}$$

Assuming that the probability of nodes i and j being infected at $t-\tau$ is independent, we have

$$\begin{aligned} \mathbb{E}\left[1_{\{x_i(t-\tau)=1\}} 1_{\{x_j(t-\tau)=1\}}\right] &= \mathbb{E}\left[1_{\{x_i(t-\tau)=1\} \cap \{x_j(t-\tau)=1\}}\right] \\ &= \Pr\left(x_i(t-\tau)=1, x_j(t-\tau)=1\right) \\ &= \Pr\left(x_i(t-\tau)=1\right) \Pr\left(x_j(t-\tau)=1\right), \end{aligned} \tag{2.5}$$

which then yields the following delayed Markov differential equation for node i:

$$\begin{cases} \dot{p}_i(t) = -\delta p_i(t-\tau) + \beta(1 - p_i(t-\tau)) \sum_{j=1}^{n} a_{ij} p_j(t-\tau);\ t \geq \tau, \\ p_i(t) = \phi_i(t);\ t \leq \tau, \end{cases} \tag{2.6}$$

where $p_i(t-\tau) = \mathbb{E}[q_i(t-\tau)] = \Pr(x_i(t-\tau)=1)$, $p_j(t-\tau) = \mathbb{E}[q_j(t-\tau)] = \Pr(x_j(t-\tau)=1)$, and $\phi_i(t)$ is the initial history function of infection for node i. This approximation is valid for small values of infection rate and time step.

Using (2.6), the n-intertwined SIS model of network can now be expressed as

$$\begin{cases} \dot{\mathbf{p}}(t) = \mathcal{A}\mathbf{p}(t-\tau) - \beta P(t-\tau) A \mathbf{p}(t-\tau);\ t \geq \tau, \\ \mathbf{p}(t) = \boldsymbol{\phi}(t);\ t \leq \tau, \end{cases} \tag{2.7}$$

where $\mathbf{p}(t) = [p_1(t), \ldots, p_n(t)]^\top$, and $\boldsymbol{\phi}(t) = [\phi_1, \ldots, \phi_n]^\top$ is the vector of history function and $P(t-\tau) = \operatorname{diag}(\mathbf{p}(t-\tau))$. A is the nonnegative adjacency matrix of network defined in subsection 2.1, which can be decomposed by $A = VUV^\top$, where $V = [\mathbf{v}_1, \mathbf{v}_2, \ldots, \mathbf{v}_n]$ is an orthogonal matrix and $U = \operatorname{diag}([u_1, u_2, \ldots, u_n])$. $\mathcal{A}$ is obtained by $\mathcal{A} = \beta A - \delta I_n$, and its eigenvalues are denoted by $\lambda_1 \leq \lambda_2 \leq \cdots \leq \lambda_n$. The eigenvalues of adjacency matrix A can therefore be found by $u_i = \frac{\lambda_i + \delta}{\beta}$ for all $i \in \mathcal{V}$.

Remark 2.1. To evaluate the precision of the mean-field approximation applied to the probabilistic delayed SIS model discussed in this section, we compare the stochastic dynamics

Algorithm 2.1 Probabilistic delayed SIS model with fully connected graph and mean-field approximation.

Initialize
  A: Adjacency matrix, n: Number of nodes, β: Infection rate, δ: Recovery rate, T: Simulation time, Δt: Time interval, τ: Time delay, $x(i, 0:\tau)$: State history of node i for $0 \le t \le \tau$
for $t \leftarrow \tau$ to T **do**
  for $i \leftarrow 1$ to n **do**
    if $x(i,t) = 0$ **then**
      Compute *sum_check* to consider time delay effect on the infection process
      for $j \leftarrow 1$ to n **do**
        if $x(j, t-\tau) = 1$ and *sum_check* $= 0$ **then**
          if rand() $< \beta \cdot A(i,j) \cdot \Delta t$ **then**
            $x(i, t+\Delta t) = 1$
            Break
          end if
        end if
      end for
    else
      Compute *product_check* to consider time delay effect in the recovery process
      if rand() $< \delta \cdot \Delta t$ and *product_check* $= 1$ **then**
        $x(i, t+\Delta t) = 0$
      else
        $x(i, t+\Delta t) = 1$
      end if
    end if
  end for
  Update x_T, total number of infected individuals during $[0, t]$
end for
Compute total number of infected individuals during $[0, T]$ by mean-field approximation, p_T, using (2.7)
Plot x_T and p_T over time

governed by (2.1) and (2.2) with the deterministic dynamics described by (2.7), for a single population comprising n individuals. Algorithm 2.1 outlines the steps we followed to obtain the results for the probabilistic model.

In this algorithm, we incorporate the influence of time delay associated with the infection process by calculating the probability of $x(i, t-\tau) = x(i, t-\tau+\Delta t) = \cdots = x(i,t) = 0$, denoted as *sum_check*. Thus, if *sum_check* $= 0$, it indicates that node i has remained susceptible during the time interval $[t-\tau, t]$. Consequently, node i has the potential to transition to an infectious state at time $t + \Delta t$. Additionally, we account for the impact of time delay related

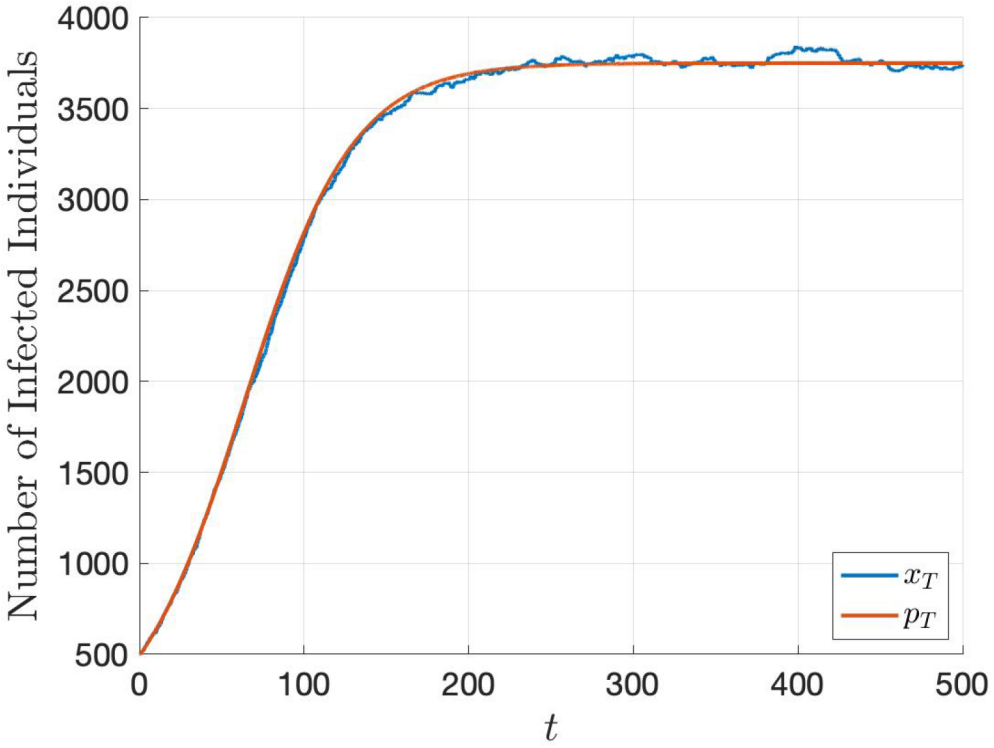

Figure 1. *Total expected number of infected individuals over time for a fully connected network with* $n = 5000$, $\beta = 0.04$, $\delta = 0.01$, *and* $\tau = 0.5$. *The blue line represents the expected number of infected individuals, while the red line corresponds to the number of infected individuals obtained using the mean-field model. Simulation time and time step are* $T = 500$, $\Delta t = 0.05$, *respectively.*

to the recovery process by calculating the probability of node i remaining infected during the time interval $[t-\tau, t]$, which is denoted as *product_check*. If *product_check* $= 1$ for node i, it indicates that node i has remained infected throughout that time interval. As a result, node i has the potential to recover and transition to a susceptible state at time $t + \Delta t$.

Figures 1 and 2 depict the number of infected individuals over time in a population with individuals interacting through a complete network with no self-loops. The simulation parameters for Figure 1 are specified as $n = 5000$, $T = 500$, $\Delta t = 0.05$, $\beta = 0.04$, $\delta = 0.01$, and $\tau = 0.5$, and for Figure 2 are specified as $n = 100$, $T = 2500$, $\Delta t = 0.05$, $\beta = 0.04$, $\delta = 0.01$, and $\tau = 50$. In both figures, the blue line corresponds to the expected value of infected individuals, denoted by x_T, which is computed as the sum of the expected values of the indicator random variable $q_i(t)$ over all nodes $i \in \{1, 2, \ldots, n\}$ and times $t \in \{0, \Delta t, 2\Delta t, \ldots, T\}$, i.e., $x_T = \sum_{t=0}^{T} \sum_{i=1}^{n} \mathbb{E}[q_i(t)]$. The red line represents the number of infected individuals predicted by the mean-field model, denoted by p_T, which is obtained as the sum of the probabilities of infection $p_i(t)$ over all nodes $i \in \{1, 2, \ldots, n\}$ and times $t \in \{0, \Delta t, 2\Delta t, \ldots, T\}$, i.e., $p_T = \sum_{t=0}^{T} \sum_{i=1}^{n} p_i(t)$.

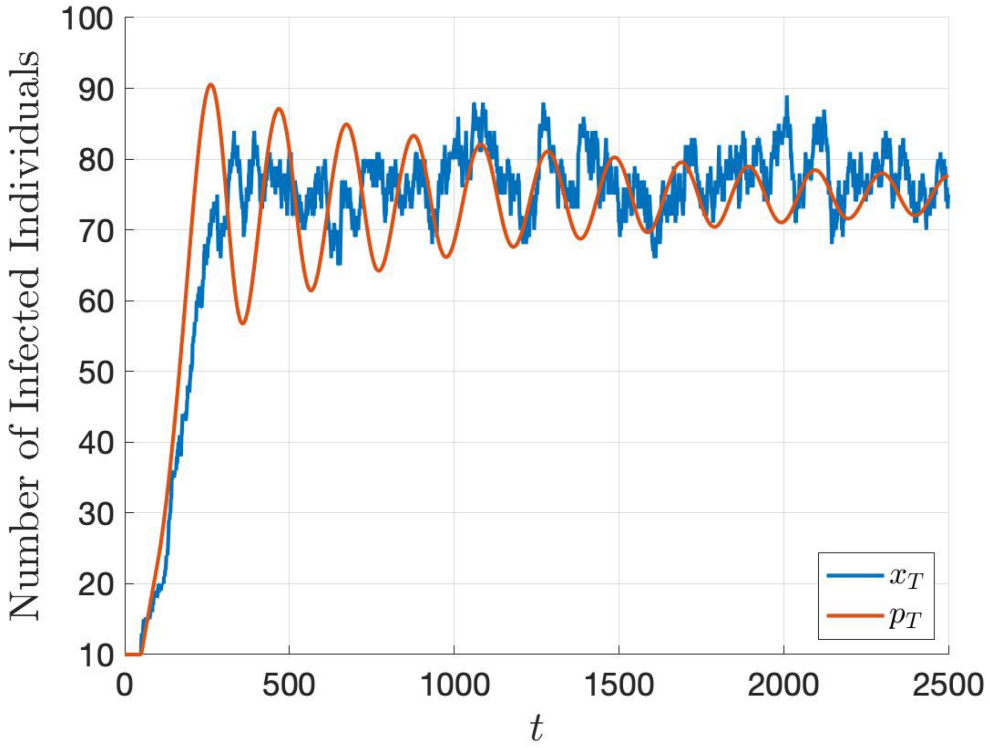

Figure 2. *Total expected number of infected individuals over time for a fully connected network with $n = 100$, $\beta = 0.04$, $\delta = 0.01$, and $\tau = 50$. The blue line represents the expected number of infected individuals, while the red line corresponds to the number of infected individuals obtained using the mean-field model. Simulation time and time step are $T = 2500$, $\Delta t = 0.05$, respectively.*

Linearization of (2.6) around its disease-free equilibrium, $p_i^*(t) = 0$ gives the following linear SIS dynamics [19]:

$$\begin{cases} \dot{p}_i(t) = -\delta p_i(t-\tau) + \beta \sum_{j=1}^{n} a_{ij} p_j(t-\tau); \ t \geq \tau, \\ p_i(t) = \phi_i(t); \ t \leq \tau. \end{cases} \tag{2.8}$$

The above linear dynamics can be expressed by the following compact form:

$$\begin{cases} \dot{\mathbf{p}}(t) = \mathcal{A}\mathbf{p}(t-\tau); \ t \geq \tau, \\ \mathbf{p}(t) = \boldsymbol{\phi}(t); \ t \leq \tau. \end{cases} \tag{2.9}$$

The basic reproduction number of an epidemic network, $\mathcal{R}_{0M}$, is a metric that provides the expected number of neighbors that an infected subpopulation will infect. For a metapopulation with dynamics (2.9), the network reproduction number is defined as

$$\mathcal{R}_{0M} := 1 + \frac{\lambda_n}{\delta}. \tag{2.10}$$

It was previously shown that for the delay-free version of epidemic network (2.9), an initial infection will converge to zero if $\mathcal{R}_{0M} < 1$ [51], which is equivalent to

$$\lambda_n \leq -\epsilon, \ \epsilon > 0, \tag{2.11}$$

for an undirected network with λ_n being the largest eigenvalue of $\mathcal{A}$. This condition guarantees the existence of an $\alpha > 0$ that satisfies $\|p_i(t)\| \leq \alpha \|p_i(0)\| e^{-\epsilon t}$, and, as a result, the disease-free equilibrium of the system will be globally exponentially stable with the rate of ϵ [48].

The basic reproduction number of subpopulation i, on the other hand, determines the progress of disease within that single population, which is found by

$$\mathcal{R}_{0S}(i) := \frac{\beta a_{ii}}{\delta}. \tag{2.12}$$

where for $\mathcal{R}_{0S}(i) < 1$ for all $i \in \mathcal{V}$, the infection size will eventually converge to zero.

The investigation of stability in delayed LTI systems is challenging due to the existence of infinitely many characteristic roots. One approach towards extracting the delay-dependent stability regions of such systems is the conversion of time delay domain such that the exponential terms in the characteristic equation are eliminated. This conversion allows us to evaluate the behavior of system by its finite characteristic roots in an alternative domain. This approach is implemented by the Rekasius substitution [54] in [14], where it is shown that for a network with dynamics (2.9) and $\mathcal{R}_{0M} < 1$, if $0 < \tau < -\frac{\pi}{2\lambda_1}$, then the asymptotic stability is guaranteed. The same result can be obtained by implementing frequency domain analysis on dynamics (2.9) [44].

Combining conditions (2.11) and (2.2) results in the following matrix inequality with respect to the positive semidefinite cone $\mathbb{S}_+^n$,

$$\epsilon I_n \preceq -\mathcal{A} \preceq \frac{\pi}{2\tau} I_n, \tag{2.13}$$

where I_n is the identity matrix of size n.

Remark 2.2. We consider the following examples to better demonstrate the impact of internal time delays and interpopulation connections on the epidemic behavior of systems with dynamics (2.7).

a. Consider a group of individuals in a closed population, indicated by the number 1. These individuals may only have contact with other individuals inside population 1, and there are no internal time delays involved. Starting from any initial infection, e.g., complete infection ($p_1(0) = 1$), for $\mathcal{R}_{0S} = 2$, a smooth transition to an endemic with $p_1(\infty) \to 0.5$ is expected. Given the properties of SIS dynamics (2.7), no peak of infection appears in this case; see Figure 3(a).

b. Consider population 1 when it is experiencing $\tau = 25$ days of delay in the process of spreading the disease among its members, who may only have contact with other individuals inside population 1. While the steady-state properties of the network remain unchanged, its transient behavior is different due to the presence of time delay; see Figure 3(b).

c. Consider two connected subpopulations 1 and 2 with no intrapopulation social distancing, i.e., $a_{ij} = 1$ for $i, j \in \{1, 2\}$. With no time delays in the epidemic network, $\tau = 0$, even if 1 and 2 stay connected, there will be no fluctuations in their infection size, see Figure 3(c).

d. Consider two connected subpopulations 1 and 2 with time delay $\tau = 25$ days. If 1 gets infected by the infectious subpopulation 2 at time t, it will become infectious at

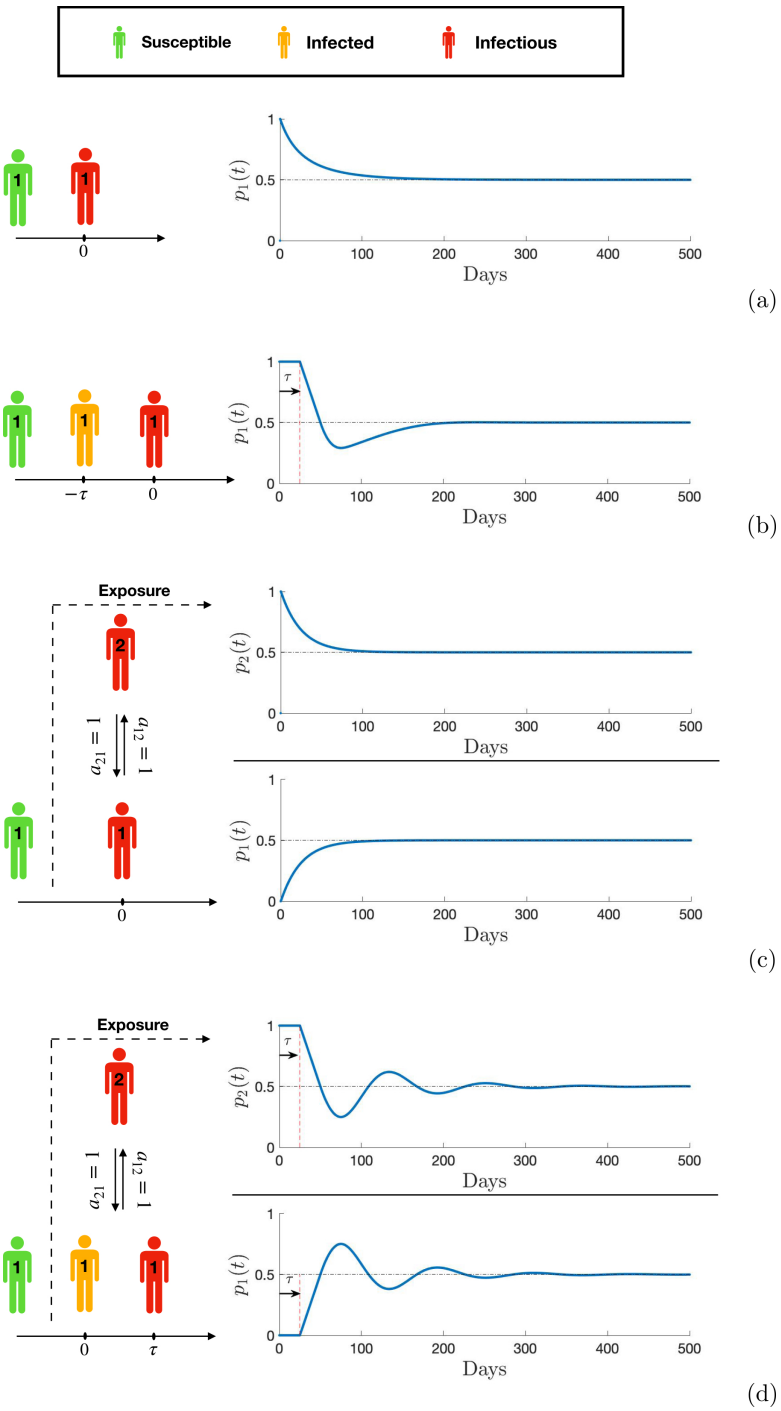

Figure 3. *Epidemic spread in* (a) *a single population with no time delay and* $\mathcal{R}_{0S} = 2$*;* (b) *a single population with time delay* $\tau = 25$ *days and* $\mathcal{R}_{0S} = 2$*;* (c) *a network of two subpopulations with no time delay and* $\mathcal{R}_{0M} = 2$*; and* (d) *a network of two subpopulations with time delay* $\tau = 25$ *days and* $\mathcal{R}_{0M} = 2$*.* p_1 *and* p_2 *denote the fraction of infectious individuals in subpopulations* 1 *and* 2*, respectively.*

time $t+\tau$, and both subpopulations will experience multiple epidemic waves before the disease reaches a steady state; see Figure 3(d).

Although for all cases above the steady-state epidemic behavior remains the same (due to an equal reproduction number), ignoring internal time delays or network effect substantially underestimates the peak of infection as well as the transient behavior of the epidemic.

3. Performance analysis in the presence of small shocks. In this section, we investigate the performance deterioration of linear network (2.9) subject to small shocks. We model the effect of shock on the infection dynamics of subpopulation i by an additive white noise such that $\xi_i(t) \sim \mathcal{N}(0,\sigma_i^2)$ and assume that the input noise for each subpopulation is independent of the others [22, 59, 60], i.e., $\boldsymbol{\xi}(t) = [\xi_1(t),\xi_2(t),\dots,\xi_n(t)]^\top$, where $\boldsymbol{\xi}(t) \sim \mathcal{N}\left(\mathbf{0}_n, \operatorname{diag}\left([\sigma_1^2,\sigma_2^2,\dots,\sigma_n^2]\right)\right)$. In what follows, the performance and robustness of network (2.9) in the presence of such external disturbances are studied. An $\mathcal{H}_2$-based performance measure is adopted from [59] to find an explicit representation for the network performance loss, which will then be utilized for optimal traffic restriction purposes in the following sections. This $\mathcal{H}_2$ norm-based measure quantifies fluctuations in the average number of infected people based on the steady-state variance of nodal state fluctuations.

Assume that the exogenous noise input described earlier is affecting the dynamics of network (2.9) as

$$\begin{cases} \dot{\mathbf{p}}(t) = \mathcal{A}\mathbf{p}(t-\tau) + \boldsymbol{\xi}(t);\ t \geq \tau, \\ \mathbf{p}(t) = \boldsymbol{\phi}(t);\ t \leq \tau. \end{cases} \tag{3.1}$$

The $\mathcal{H}_2$ norm-based performance measure, ρ_{ss}, of network (3.1) can then be found by

$$\rho_{\text{ss}} = \lim_{t\to\infty} \mathbb{E}\left[\mathbf{p}(t)^\top \mathbf{p}(t)\right], \tag{3.2}$$

where ρ_{ss} measures the performance loss of the network; therefore, smaller values of ρ_{ss} result in better performance. More details on the performance measure of a class of consensus networks under the influence of exogenous white noises can be found in the reference papers [6, 23, 60, 73]. According to [16], the performance of a stable system with transfer function $G(j\omega)$ can be found by the frequency domain definition of its $\mathcal{H}_2$ norm as follows:

$$\rho_{\text{ss}} = \frac{1}{2\pi} \operatorname{Tr}\left[\int_{-\infty}^{+\infty} G^{\text{H}}(j\omega) G(j\omega) d\omega\right], \tag{3.3}$$

where $G^{\text{H}}(j\omega)$ corresponds to the complex conjugate transpose of $G(j\omega)$. For the network system with dynamics (3.1), we define $\hat{\xi}_i := \frac{\xi_i}{\sigma_i}$ for all $i \in \mathcal{V}$. We then have

$$\boldsymbol{\xi} = B\hat{\boldsymbol{\xi}}, \tag{3.4}$$

where $\hat{\boldsymbol{\xi}} = [\hat{\xi}_1, \hat{\xi}_2, \dots, \hat{\xi}_n]$ and $B = \operatorname{diag}([\sigma_1,\sigma_2,\dots,\sigma_n])$. Note that $\hat{\boldsymbol{\xi}}$ is a vector of unit variance and identically distributed Gaussian processes. Next, we define $G(j\omega)$ as the transfer function from $\hat{\boldsymbol{\xi}}(t)$ to $\mathbf{p}(t)$ and present the following lemma.

Lemma 3.1. *For epidemic network* (3.1) *the closed form solution of* (3.3) *is*

$$\rho_{ss} = \sum_{i=1}^{n} -\frac{\Phi_i}{2\lambda_i} \frac{\cos(\lambda_i \tau)}{1+\sin(\lambda_i \tau)}, \tag{3.5}$$

in which Φ_i *is the* ith *diagonal element of the matrix* $Q^\top BB^\top Q$, *where* $Q = [\mathbf{q}_1, \ldots, \mathbf{q}_n] \in \mathbb{R}^{n\times n}$ *is the orthonormal matrix of eigenvectors of* $\mathcal{A}$. λ_i *for all* $i \in \mathcal{V}$ *is the* ith *eigenvalue of matrix* $\mathcal{A}$.

Proof. The transfer matrix of (3.1) from input noise to state is defined as

$$\begin{aligned} G(j\omega) &= \left(j\omega I_n - e^{-j\tau\omega}\mathcal{A}\right)^{-1} B \\ &= Q\,\mathrm{diag}\left(\left[\frac{1}{j\omega - \lambda_1 e^{-j\tau\omega}}, \cdots, \frac{1}{j\omega - \lambda_n e^{-j\tau\omega}}\right]\right) Q^\top B. \end{aligned} \tag{3.6}$$

For this transfer matrix we have

$$\mathrm{Tr}\left[G^{\mathrm{H}}(j\omega)G(j\omega)\right] = \mathrm{Tr}\left[Q^\top BB^\top Q D(j\omega)D(-j\omega)\right], \tag{3.7}$$

where $D(j\omega) = \mathrm{diag}([\frac{1}{-\lambda_1 e^{j\tau\omega} - j\omega}, \cdots, \frac{1}{-\lambda_n e^{j\tau\omega} - j\omega}])$.

Substituting (3.7) into (3.3), the performance measure will be

$$\rho_{\mathrm{ss}} = \frac{1}{2\pi} \sum_{i=1}^{n} \int_{-\infty}^{+\infty} \frac{\Phi_i d\omega}{(j\omega + \lambda_i e^{j\tau\omega})(\lambda_i e^{-j\tau\omega} - j\omega)}. \tag{3.8}$$

A proof follows by solving the integration above and finding the summation of its solution for all the n nodes of the network. ∎

Remark 3.2. The squared $\mathcal{H}_2$ norm of an exponentially stable delayed network (3.1) can be calculated as the energy functional (3.2), where $\mathbf{p}(t)$ is the response to the Gaussian white noise $\xi_i(t) \sim \mathcal{N}(0, \sigma_i^2)$ with $\sigma_i = 1$ for all $i \in \mathcal{V}$. This metric (3.3) can also be interpreted as the impulse response energy, ρ_{ss}, which quantifies the L_2 norm of the number of daily infected cases; in this case, $\xi_i(t)$ is the Dirac delta function, a.k.a. the unit impulse. We should note that ρ_{ss} measures the performance loss of the network; therefore, smaller values of ρ_{ss} result in better performance.

4. Epidemic-based centrality index.

In this section, we focus on an epidemic network where subpopulation-level shocks remain small. This assumption allows us to linearize the network's noisy dynamics around its disease-free equilibrium. A subpopulation's impact on disease propagation depends on its strategic location in the epidemic network, which can be captured using traditional node centralities. However, factors such as epidemic rates and internal time delays can also influence a node's contribution to disease propagation, which traditional centralities cannot capture. To address this, we introduce an epidemic-based centrality index using the performance measure introduced earlier. We use this index to rank subpopulations based on their contribution to network robustness against an exogenous disturbance/shock. In the following, we provide a formal definition for our epidemic-based centrality measure.

Definition 4.1. *Consider system (3.1) with an additive Gaussian white noise, $\xi_i(t) \sim \mathcal{N}(0, \sigma_i^2)$ for all $i \in \mathcal{V}$. We define the epidemic-based centrality of subpopulation i by the rate of network performance measure (3.5) with respect to the following noise variance:*

$$\eta_i := \frac{\partial \rho_{ss}}{\partial \sigma_i^2}. \tag{4.1}$$

Corollary 4.2. *The epidemic-based centrality index of i^{th} subpopulation in network (3.1) is*

$$\eta_i = -\frac{1}{2}\left[\mathcal{A}^{-1}\cos(\tau\mathcal{A})\left(I_n + \sin(\tau\mathcal{A})\right)^{-1}\right]_{ii}$$

for all $i \in \mathcal{V}$. Note that $\mathcal{A} = \beta A - \delta I_n$, and operator $[.]_{ii}$ returns the ith diagonal element of its matrix argument.

Proof. Using Lemma 3.1, the performance measure can be expressed by the following compact matrix operator form:

$$\rho_{\text{ss}} = -\frac{1}{2}\operatorname{Tr}\left[BB^\top \mathcal{A}^{-1}\cos(\tau\mathcal{A})\left(I_n + \sin(\tau\mathcal{A})\right)^{-1}\right]. \tag{4.2}$$

Substituting (4.2) into (4.1), the proof is obtained. ∎

Network performance measure ρ_{ss} can now be retrieved using Corollary 4.2 as follows:

$$\rho_{\text{ss}} = \sum_{i\in\mathcal{V}} \eta_i \sigma_i^2. \tag{4.3}$$

The series expansion of epidemic-based centrality η_i can be obtained by

$$\begin{aligned}\eta_i &= -\frac{1}{2}\left[\mathcal{A}^{-1}\cos(\tau\mathcal{A})\left(I_n + \sin(\tau\mathcal{A})\right)^{-1}\right]_{ii}\\ &= c_0(\delta\tau) + \frac{\beta}{\delta}c_1(\delta\tau)[A]_{ii} + \frac{\beta^2}{\delta^2}c_2(\delta\tau)[A^2]_{ii} + \cdots\\ &= \sum_{k=0}^{\infty}\frac{\beta^k}{\delta^k}c_k(\delta\tau)[A^k]_{ii},\end{aligned} \tag{4.4}$$

where

$$c_0(\delta\tau) = \frac{\cos(\delta\tau)}{2\delta(1-\sin(\delta\tau))},\ c_1(\delta\tau) = \frac{\cos(\delta\tau)-\delta\tau}{2\delta(1-\sin(\delta\tau))},$$

and

$$c_2(\delta\tau) = \frac{2(\cos(\delta\tau)-\delta\tau)(1-\sin(\delta\tau))^2 + \delta^2\tau^2\cos(\delta\tau)(\cos(\delta\tau)-\sin(\delta\tau)+\sin^2(\delta\tau))}{4\delta(1-\sin(\delta\tau))^3}.$$

We will use the expanded form of epidemic-based centrality later.

While the proposed epidemic-based centrality considers more than just the location of nodes in the network to rank them, it is worthwhile to explore its relationship with other centralities that solely rely on the network structure (adjacency matrix). We aim to investigate whether well-known centralities like resolvent, local, and eigenvector can produce the same results as epidemic-based centrality. If so, we seek to determine the range of epidemic rates and time delays that yield similar rankings. In the subsequent subsections, we will endeavor to answer these queries.

4.1. Correlation with resolvent centrality. We define the resolvent centrality (a.k.a. resolvent subgraph centrality) of undirected network (3.1) with weighted adjacency matrix A by[1]

$$\begin{aligned} RC_i(\alpha) &= \left[(I_n - \alpha A)^{-1}\right]_{ii} \\ &= 1 + \alpha[A]_{ii} + \alpha^2[A^2]_{ii} + \cdots + \alpha^k[A^k]_{ii} + \cdots = \sum_{k=0}^{\infty} \alpha^k [A^k]_{ii}, \end{aligned} \tag{4.5}$$

where $[A]_{ii}$ indicates the weight of self-loop for node i. $[A^2]_{ii} = \sum_{i=1}^{n} a_{ij}^2$ provides the sum of weighted closed walks with length 2 starting from i. $[A^k]_{ii}$ computes the sum of weighted closed walks of length k starting from i. α is bounded from above by the inverse of A's largest eigenvalue to ensure that $I_n - \alpha A$ is invertible and that its power series converges to its inverse. Note that the largest eigenvalue of A is denoted by u_n; therefore, $0 < \alpha < \frac{1}{u_n}$. Resolvent centrality of node i presents the sum of weighted closed walks of length k for $k = 0, 1, 2, \ldots$, where weighted closed walks of length k are penalized by α^k. When the underlying graph is unweighted and has no self-loops, $RC_i(\alpha)$ counts the total number of closed walks beginning at node i while weighting walks of length k by α^k. The following theorem presents a correlation between epidemic-based and resolvent centralities.

Theorem 4.3. *For undirected epidemic network (3.1) over a weighted (or unweighted) graph $\mathcal{G}$ with adjacency matrix $A = [a_{ij}] \in \mathbb{R}^{n \times n}$, infection rate β, recovery rate δ, and time delay $\tau \to 0$, node ranking obtained by epidemic-based centrality η_i is equivalent to that provided by resolvent centrality RC_i, where $\alpha = \frac{\beta}{\delta}$.*

Proof. When $\tau \to 0$, the epidemic-based centrality reduces to

$$\begin{aligned} \lim_{\tau \to 0} \eta_i &= \lim_{\tau \to 0} -\frac{1}{2}\left[\mathcal{A}^{-1}\cos(\tau\mathcal{A})\left(I_n + \sin(\tau\mathcal{A})\right)^{-1}\right]_{ii} \\ &= -\frac{1}{2}\left[\mathcal{A}^{-1}\right]_{ii} \\ &= -\frac{1}{2}\left[(\beta A - \delta I_n)^{-1}\right]_{ii} \\ &= \frac{1}{2\delta}\left[\left(I_n - \frac{\beta}{\delta}A\right)^{-1}\right]_{ii} \\ &= \frac{1}{2\delta} RC_i\left(\frac{\beta}{\delta}\right). \end{aligned} \tag{4.6}$$

[1]The resolvent-based centrality measure, introduced by Katz [29], penalizes long walks of length k from node i through multiplication by a fixed factor α^k for each edge used, and these measures capture the ability of node i to initiate walks to all nodes in the network. Originally, Katz proposed using the row sums of $(I - \alpha A)^{-1}$ as a centrality measure $CK_i(\alpha) = \mathbf{e}_i^{\top}(I - \alpha A)^{-1}\mathbf{1}_n$, where $\mathbf{e}_i$ is the ith standard basis vector and $\mathbf{1}_n$ is the vector of all ones. However, the resolvent-based subgraph centrality [9] uses the diagonal entries of $(I - \alpha A)^{-1}$ instead.

Since RC_i is only rescaled by a constant value $\frac{1}{2\delta}$, the node ranking provided by resolvent centrality for $\alpha = \frac{\beta}{\delta}$ converges to that found by epidemic-based centrality when $\tau \to 0$. ∎

4.2. Correlation with local centralities. We define the following local centrality for epidemic network (3.1) with adjacency matrix $A = [a_{ij}]$:

$$o_i := [A]_{ii} = a_{ii}, \tag{4.7}$$

which is dependent on local social distancing status (self-loops) in the network. We also introduce another local centrality for epidemic network (3.1) as follows:

$$l_i := [A^2]_{ii} = \sum_{j=1}^{n} a_{ij}^2, \tag{4.8}$$

which returns the sum of weighted closed walks with length 2 starting from node i. Note that for an unweighted undirected network with no self-loops, l_i returns the degree centrality of node i, which is a special version of local centrality. We denote the output of rankings obtained using centrality measures η_i, o_i, and l_i by $\mathcal{I}_e$, $\mathcal{I}_o$, and $\mathcal{I}_l$, respectively. In other words, $\mathcal{I}_e$, $\mathcal{I}_o$, and $\mathcal{I}_l$ present the set of nodes ranked in descending order based on the value of their corresponding centrality index. In what follows, the reverse order of a set $\mathcal{I}$ is denoted by $\mathrm{R}(\mathcal{I})$. In the following theorem, we propose a correlation between local centralities and epidemic-based centrality when the ratio of infection rate to recovery rate is close to zero, i.e., the disease is not highly contagious.

Theorem 4.4. *For epidemic network (3.1) over a weighted undirected graph $\mathcal{G}$ with adjacency matrix $A = [a_{ij}] \in \mathbb{R}^{n\times n}$, infection rate β, recovery rate δ, and time delay $0 < \tau < \frac{\pi}{2\lambda_1}$, if $\frac{\beta}{\delta} \to 0^+$, then the following statements hold:*

(i) *When all subpopulations follow local social distancing (graph $\mathcal{G}$ with adjacency matrix A is loopless), i.e., $a_{ii} = 0$ for all $i \in \mathcal{V}$, then*

$$\mathcal{I}_e = \mathcal{I}_l. \tag{4.9}$$

(ii) *When some subpopulations follow local social distancing (graph $\mathcal{G}$ with adjacency matrix A contains loops), i.e., $a_{ii} \neq 0$ for some $i \in \mathcal{V}$, then*

$$\mathcal{I}_e = \begin{cases} \mathcal{I}_o & \text{if } \ 0 < \delta\tau < z_1, \\ \mathcal{I}_l & \text{if } \ \delta\tau = z_1, \\ \mathrm{R}(\mathcal{I}_o) & \text{if } \ z_1 < \delta\tau < \frac{\pi}{2}, \end{cases} \tag{4.10}$$

where $z_1 \approx 0.739$ is the numerical solution to $c_1(z_1) = 0$ such that $z_1 < \frac{\pi}{2}$ (see (4.4)).

Proof. According to the stability criterion (2.2), when $\frac{\beta}{\delta} \to 0^+$ the feasible range of $\delta\tau$ is $0 < \delta\tau < \frac{\pi}{2}$. In other words, for epidemic network (3.1), $\delta\tau > \frac{\pi}{2}$ results in instability when the infection rate is significantly lower than the recovery rate.

To prove (i), we define μ_i as

$$\mu_i := \frac{\delta^2}{\beta^2 c_2(\delta\tau)}[\eta_i - c_0(\delta\tau)] = 0 + [A^2]_{ii} + \frac{\beta}{\delta}\frac{c_3(\delta\tau)}{c_2(\delta\tau)}[A^3]_{ii} + \frac{\beta^2}{\delta^2}\frac{c_4(\delta\tau)}{c_2(\delta\tau)}[A^4]_{ii} + \cdots. \tag{4.11}$$

For any δ and β, node rankings based on η_i and μ_i are equal if $c_2(\delta\tau) > 0$. $c_2(\delta\tau)$, defined in (4.4), is positive for various ranges of $\delta\tau$; however, only $0 < \delta\tau < \frac{\pi}{2}$ belongs to the range of stability found by (2.2). Thus, when $\frac{\beta}{\delta} \to 0^+$, the rankings based on η_i and μ_i are always equal. When $\frac{\beta}{\delta} \to 0^+$, we have

$$\lim_{\frac{\beta}{\delta}\to 0^+} \mu_i = [A^2]_{ii} = \sum_{j=1}^{n} a_{ij}^2 = l_i, \tag{4.12}$$

which results in (4.9).

To prove (ii), we define $\gamma_i := \frac{\delta}{\beta c_1(\delta\tau)}[\eta_i - c_0(\delta\tau)]$ as a centrality index for ranking network nodes. The centrality of node i based on γ_i index is then obtained by

$$\gamma_i = \frac{\delta}{\beta c_1(\delta\tau)}[\eta_i - c_0(\delta\tau)] = [A]_{ii} + \frac{\beta}{\delta}\frac{c_2(\delta\tau)}{c_1(\delta\tau)}[A^2]_{ii} + \frac{\beta^2}{\delta^2}\frac{c_3(\delta\tau)}{c_1(\delta\tau)}[A^3]_{ii} + \cdots, \tag{4.13}$$

which yields

$$\lim_{\frac{\beta}{\delta}\to 0^+} \gamma_i = [A]_{ii} = a_{ii} = o_i. \tag{4.14}$$

For any δ and β, node rankings based on η_i and γ_i are equal if $c_1(\delta\tau) > 0$, since η_i is only scaled by a constant positive value and shifted by a constant value. Combining conditions $c_1(\delta\tau) > 0$ and $0 < \delta\tau < \frac{\pi}{2}$, returns $0 < \delta\tau < z_1$, where $z_1 \approx 0.739$, as the only feasible range for $\delta\tau$. We therefore have $\mathcal{I}_e = \mathcal{I}_o$ for $0 < \delta\tau < z_1$.

If $c_1(\delta\tau) < 0$, then a reverse order of ranking will be provided by γ_i, which happens only for $z_1 < \delta\tau < \frac{\pi}{2}$, $z_1 \approx 0.739$. We therefore have $\mathcal{I}_e = \mathrm{R}(\mathcal{I}_o)$ for $z_1 < \delta\tau < \frac{\pi}{2}$.

In a more specific case when $\delta\tau = z_1$, the first and second terms in (4.4) are zero, and the same procedure as in the proof of part (i) can be followed, which yields $\mathcal{I}_e = \mathcal{I}_l$. ∎

As a result of this theorem, when all the subpopulations follow local social distancing, and the infection rate is comparatively low with respect to recovery rate, instead of an epidemic-based ranking, the local ranking l_i can be used to reduce the computation complexities. In other words, for network (3.1), when the spreading disease is not highly contagious, using local centralities to identify the central nodes is sufficient.

Similarly, the output of epidemic-based centrality, $\mathcal{I}_e$, and the output of local centralities, $\mathcal{I}_o$ and $\mathcal{I}_l$, can be used interchangeably based on (4.10) when some subpopulations do not follow local social distancing guidelines and the infection rate is comparatively low with respect to recovery rate.

4.3. Correlation with eigenvector centrality. The eigenvector centrality for epidemic network (3.1) with adjacency matrix $A = [a_{ij}]$ is obtained by

$$ev_i := \mathbf{e}_i^\top \mathbf{v}_n = \mathbf{v}_n(i), \tag{4.15}$$

where $\mathbf{e}_i$ is the ith standard basis vector, and $\mathbf{v}_n$ is the dominant eigenvector of matrix A associated with its largest eigenvalue u_n. Since network (3.1) is undirected, we can decompose its nonnegative adjacency matrix by $A = VUV^\top$, where $V = [\mathbf{v}_1, \mathbf{v}_2, \ldots, \mathbf{v}_n]$ is orthogonal and

$U = \text{diag}([u_1, u_2, \ldots, u_n])$. Note that, based on the Perron–Frobenius theorem, a connected graph with nonnegative adjacency matrix A has a nonnegative real eigenvalue, which has the maximum absolute value among all eigenvalues, that is, $|u_1| \leq \cdots \leq |u_{n-1}| < u_n$. The eigenvector associated with u_n can be chosen to have nonnegative real entries, i.e., $\mathbf{v}_n > 0$.

We denote the output of node ranking based on eigenvector centrality ev_i by $\mathcal{I}_{ev}$ and present the following theorem to connect the epidemic-based centrality and eigenvector centrality for certain ranges of epidemic rates.

Theorem 4.5. *For epidemic network (3.1) over a weighted undirected graph $\mathcal{G}$ with adjacency matrix $A = [a_{ij}] \in \mathbb{R}^{n\times n}$, infection rate β, recovery rate δ, and time delay $\tau \to 0^+$, if $\frac{\beta}{\delta} \to \frac{1}{u_n}^-$, the ranking provided by epidemic-based centrality, $\mathcal{I}_e$, converges to that obtained by eigenvector centrality, $\mathcal{I}_{ev}$.*

Proof. For undirected network (3.1), the diagonal elements of the kth power of its adjacency matrix can be obtained in terms of its eigenvalues and eigenvectors as follows:

$$[A^k]_{ii} = \sum_{j=1}^{n} u_j^k \mathbf{v}_j^2(i), \tag{4.16}$$

where u_j and $\mathbf{v}_j$ are the jth eigenvalue and normalized eigenvector of A, respectively. $\mathbf{v}_j(i)$ corresponds to the ith entry of $\mathbf{v}_j$.

Based on (4.4), as $\tau \to 0^+$ we have $c_k(\delta\tau) \to \frac{1}{2\delta}$. Using (4.16) in (4.4) with $\tau \to 0^+$, we have the following expansion of epidemic-based centrality:

$$\begin{aligned} \lim_{\tau\to 0^+} \eta_i &= \sum_{k=0}^{\infty} \frac{\beta^k}{2\delta^{k+1}} \sum_{j=1}^{n} u_j^k \mathbf{v}_j^2(i) \\ &= \sum_{j=1}^{n} \sum_{k=0}^{\infty} \frac{\beta^k}{2\delta^{k+1}} u_j^k \mathbf{v}_j^2(i). \end{aligned} \tag{4.17}$$

The internal summation with respect to index k can be defined as $\sum_{k=0}^{\infty} \frac{\beta^k}{2\delta^{k+1}} u_j^k = \text{f}(\beta, \delta, u_j)$. η_i is then expressed as

$$\begin{aligned} \lim_{\tau\to 0^+} \eta_i &= \sum_{j=1}^{n} \text{f}(\beta, \delta, u_j) \mathbf{v}_j^2(i) \\ &= \text{f}(\beta, \delta, u_n) \mathbf{v}_n^2(i) + \sum_{j=1}^{n-1} \text{f}(\beta, \delta, u_j) \mathbf{v}_j^2(i). \end{aligned} \tag{4.18}$$

Next, we define

$$\psi_i := \frac{1}{\text{f}(\beta, \delta, u_n)} \lim_{\tau\to 0^+} \eta_i = \mathbf{v}_n^2(i) + \sum_{j=1}^{n-1} \frac{\text{f}(\beta, \delta, u_j)}{\text{f}(\beta, \delta, u_n)} \mathbf{v}_j^2(i). \tag{4.19}$$

Note that for $u_n > 0$, $\text{f}(\beta, \delta, u_n) > 0$. Thus, when $\tau \to 0^+$, ξ_i will provide same ranking results as η_i, given that the centrality measures produced by η_i are all rescaled by the same

positive value $\frac{1}{\mathrm{f}(\beta,\delta,u_n)}$. We now apply the result of Lemma 3 in [9] to find ψ_i as $\frac{\beta}{\delta} \to \frac{1}{u_n}^-$. The radius of convergence, R, for series $\mathrm{f}(\beta,\delta,u_j)$ is $R = |\frac{\delta}{\beta}|$, which converges to u_n^+ as $\frac{\beta}{\delta} \to \frac{1}{u_n}^-$. Since $u_n > |u_j|$ for $j = 1, 2, \ldots, n-1$, $|u_j| < R$; therefore we have

$$\lim_{\frac{\beta}{\delta} \to \frac{1}{u_n}^-} \frac{\mathrm{f}(\beta,\delta,u_j)}{\mathrm{f}(\beta,\delta,u_n)} = 0 \quad \text{for } j = 1, 2, \ldots, n-1, \tag{4.20}$$

which leads to

$$\lim_{\frac{\beta}{\delta} \to \frac{1}{u_n}^-} \psi_i = \mathbf{v}_n^2(i). \tag{4.21}$$

Since $\mathbf{v}_n(i) > 0$, it will produce the same node rankings as $\mathbf{v}_n^2(i)$. According to (4.15), $\mathbf{v}_n(i)$ also provides the eigenvector centrality for network (3.1). We therefore conclude that if network (3.1) is not experiencing delays, then $\mathcal{I}_e \to \mathcal{I}_{ev}$ as $\frac{\beta}{\delta} \to \frac{1}{u_n}^-$. ∎

Theorems 4.3 and 4.5 demonstrate that resolvent centrality and eigenvector centrality only consider epidemic rates for node ranking when there is no delay. This limitation significantly reduces the applicability of these centralities in many epidemic processes that involve delay.

4.4. Interlacing nodes in epidemic-based centrality. The purpose of this subsection is to investigate the effect of disease characteristics on the epidemic-based node ranking of network (2.9) when $\tau = 0$. As shown in the previous subsections, rankings obtained by epidemic-based centrality are subject to change when different types of infections are considered or when epidemic properties of a certain disease undergo slow changes over time. The interlacing problem for a special case is studied in this subsection. Note that this subsection does not consider time-varying epidemic parameters or a linear time-varying (LTV) system but only involves an interlacing analysis for network (3.1) when $\tau = 0$.

Definition 4.6. *Two nodes i and j of graph $\mathcal{G}$ are cospectral if for every integer $k \geq 0$, we have $[A^k]_{ii} = [A^k]_{jj}$.*[2]

Definition 4.7. *Two noncospectral nodes i and j of graph $\mathcal{G}$ interlace at $\frac{\beta}{\delta}$ if $\eta_i|_{\frac{\beta}{\delta}} = \eta_j|_{\frac{\beta}{\delta}}$; $\frac{\beta}{\delta}$ is an interlacing value.*

We should note that two cospectral nodes also have the same degree, eigenvector, and epidemic-based centrality measures. The following theorem provides an upper bound on the number of interlacing values for every pair of nodes in the nondelayed version of network (3.1) when epidemic-based centrality is incorporated.

Theorem 4.8. *Consider the epidemic network (3.1) over graph $\mathcal{G}$. When $\tau = 0$, for any two noncospectral nodes $i, j \in \mathcal{V}$, there can be at most $n-1$ interlacing values for epidemic-based centrality.*

[2]Equivalently, two vertices i and j in a graph $\mathcal{G}$ are cospectral if the node-removed subgraphs $\mathcal{G}\backslash\{i\}$ and $\mathcal{G}\backslash\{j\}$ have the same characteristic polynomial (cf. [9, 24]).

Proof. We use contradiction to prove this theorem. Using Cramer's rule, we have

$$\eta_i\Big|_{\tau=0} = \frac{1}{2\delta}\left[\left(I_n - \frac{\beta}{\delta}A\right)^{-1}\right]_{ii} = \frac{1}{2\delta}\frac{\det\left(I_n - \frac{\beta}{\delta}A_{[ii]}\right)}{\det\left(I_n - \frac{\beta}{\delta}A\right)}, \tag{4.22}$$

where $A_{[ii]}$ is found by removing the ith row and column of A. Next, we define $g(\frac{\beta}{\delta}) := \eta_i|_{\tau=0} - \eta_j|_{\tau=0}$ and use Cramer's rule as follows:

$$g\left(\frac{\beta}{\delta}\right) = \frac{1}{2\delta}\frac{\det\left(I_n - \frac{\beta}{\delta}A_{[ii]}\right) - \det\left(I_n - \frac{\beta}{\delta}A_{[jj]}\right)}{\det\left(I_n - \frac{\beta}{\delta}A\right)}. \tag{4.23}$$

Assume that there can be n or more interlacing values for any two noncospectral nodes $i, j \in \mathcal{V}$ when nondelayed epidemic-based centrality is considered. In other words, there are at least n pairs of (β, δ) that satisfy $g(\frac{\beta}{\delta}) = 0$, which consists of two polynomials of degree $n-1$ in $\frac{\beta}{\delta}$. If (4.23) has n or more zeros, then the two polynomials of degree $n-1$ coincide in n or more points, which means they are identical polynomials with equivalent coefficients, i.e., when $\tau = 0$, $\eta_i = \eta_j$ for any $\frac{\beta}{\delta}$. On the other hand, based on

$$\eta_i\Big|_{\tau=0} = \frac{1}{2\delta}\left[\left(I_n - \frac{\beta}{\delta}A\right)^{-1}\right]_{ii} = \frac{1}{2\delta} + \frac{\beta}{2\delta^2}[A]_{ii} + \frac{\beta^2}{2\delta^3}[A^2]_{ii} + \frac{\beta^3}{2\delta^4}[A^3]_{ii} + \cdots, \tag{4.24}$$

$\delta\eta_i$ and $\delta\eta_j$ are polynomials of $\frac{\beta}{\delta}$ with kth coefficient as $[A^k]_{ii}$ and $[A^k]_{jj}$, respectively. This therefore implies that if $\eta_i = \eta_j$, then $[A^k]_{ii} = [A^k]_{jj}$ for any $k \geq 0$, which means i and j are cospectral (see Definition 4.6). This contradicts our assumption; therefore, there must be at most $n-1$ interlacing values for nodes i and j when epidemic-based centrality is applied. ∎

5. Epidemic containment by traffic flow optimization.

Monitoring and regulation of traffic volume are some of government interventions enacted to potentially mitigate an epidemic threat. Regarding the underlying epidemiological network, traffic restriction between two subpopulations i and j will directly modify their corresponding edge weight, $w_e = a_{ij}$. Therefore, the stability around a disease-free state can be obtained by monitoring and management of the transportation network and traffic volume restriction between the highly infectious and highly susceptible subpopulations. In this section, we propose two approaches for traffic restriction in a metapopulation with noisy and delayed linear SIS dynamics (3.1).

5.1. Optimal traffic restriction.

Consider a delayed epidemic network with dynamics (3.1) which is experiencing a normal distribution of input noise in all of its nodes, i.e., $\sigma_i \sim \mathcal{N}(0,1)$ for $i = 1, 2, \ldots, n$ (which means $B = I_n$ in (4.2)). This external noise/shock might originate from modifications in the transportation network, which are not modeled in the dynamics. The goal is to design a traffic restriction policy to prevent network performance deterioration due to exogenous noises and time delay. In this regard, the following traffic optimization method is designed to determine the optimal traffic flow between the nodes by reducing network performance loss, ρ_{ss}:

$$
\begin{aligned}
&\underset{w_e,\forall e\in\mathcal{E}}{\text{minimize}} \quad \rho_{\text{ss}} \\
&\text{subject to } \underline{w}_e \le w_e \le \overline{w}_e, \\
&\qquad \sum_{e\in\mathcal{E}} w_e = c, \\
&\qquad \mathcal{A} = \beta \sum_{e\in\mathcal{E}} w_e A_e + \beta \text{diag}\,(A) - \delta I_n, \\
&\qquad -\frac{\pi}{2\tau} I_n \preceq \mathcal{A} \preceq -\epsilon I_n.
\end{aligned} \tag{5.1}
$$

Here, the first constraint determines the lower and upper bounds on the edge weights of the network. This constraint is to ensure the resulting traffic volume between a pair of subpopulations is not less than a certain volume, $\underline{w}_e$, that is imposed by economic considerations, for instance. It also does not let the resulting traffic flow exceed a certain capacity, $\overline{w}_e$. The second constraint determines the total weight of network edges or the *overall traffic volume,* which might acquire any desired value, c, depending on the intensity of isolation. Smaller values of c are associated with conservative lockdown policies. It is preferable to keep c as close as possible to its pre-epidemic value (overall traffic volume with no restrictions) while enforcing a traffic policy to control the epidemic. The third constraint, in which A_e is the adjacency matrix of link e, provides the definition of $\mathcal{A}$ with respect to edge weights. The last constraint will guarantee that the network remains stable (see (2.13)) through the alternation of its edge weights.

In the following steps, we use convex optimization tools to solve (5.1). Let us consider a general optimization problem with the following form:

$$
\begin{aligned}
&\underset{z}{\text{minimize}} \quad f_0(z) \\
&\text{subject to } f_i(z) \le b_i, \quad i = 1,\dots,q, \\
&\qquad\qquad\quad h_i(z) = 0, \quad i = 1,\dots,r.
\end{aligned} \tag{5.2}
$$

It is considered a convex optimization problem if $f_0,\dots,f_q$ are convex functions of z and all the equality constraints $h_1,\dots,h_r$ are affine with respect to variable z [10]. According to this definition, problem (5.1) does not fall into the category of convex problems, as its cost function (see (4.2)) is nonconvex with respect to w_e. Hence, some modifications of the original optimal problem (5.2) are required to convert it into a convex optimization setup which is easier to evaluate. In this regard, an approximation of the derived performance measure in (4.2) when $B = I_n$ has been offered by [23], which converts the product of nonconvex trigonometric functions in ρ_{ss} to a linear function of $\mathcal{A}$ and its inverse. The approximated network performance measure is

$$
\rho_{\text{ss}} \simeq -\frac{1}{2}\,\text{Tr}\left[\mathcal{A}^{-1} - \frac{4\tau}{\pi}\left(\frac{\pi}{2} I_n + \tau\mathcal{A}\right)^{-1} + c_1\tau^2\mathcal{A} - \frac{c_0}{2}\tau I_n\right], \tag{5.3}
$$

where constant parameters $c_0 = 0.1873$ and $c_1 = -0.01$ are estimated to minimize the mean squared error of the approximated performance measure. Note that (5.3) is still not a convex function due to the nonconvex inverse functions $\mathcal{A}^{-1}$ and $\left(\frac{\pi}{2} I_n + \tau\mathcal{A}\right)^{-1}$. We now introduce the epigraph variables X_1 and X_2 as follows:

$$\begin{aligned} &\mathcal{A}^{-1} - X_1 \preceq 0, \\ &\left(\frac{\pi}{2} I_n + \tau \mathcal{A}\right)^{-1} - X_2 \preceq 0. \end{aligned} \tag{5.4}$$

The inequalities are convertible into linear matrix inequalities (LMI) using the Schur complement condition for positive semidefiniteness of a block matrix [10]. Applying (5.3) and (5.4) on the optimization problem (5.1), the problem can be cast as

$$\begin{aligned} \underset{X_1; X_2; w_e, \forall e \in \mathcal{E}}{\text{minimize}} \quad & \operatorname{Tr}\left[-X_1 + \frac{4\tau}{\pi} X_2 - c_1 \tau^2 \mathcal{A}\right] \\ \text{subject to} \quad & \underline{w}_e \le w_e \le \overline{w}_e, \\ & \sum_{e \in \mathcal{E}} w_e = c, \\ & \mathcal{A} = \beta \sum_{e \in \mathcal{E}} w_e A_e + \beta \operatorname{diag}(A) - \delta I_n, \\ & -\frac{\pi}{2\tau} I_n \preceq \mathcal{A} \preceq -\epsilon I_n, \\ & \begin{bmatrix} X_1 & I_n \\ I_n & \mathcal{A} \end{bmatrix} \succeq 0, \\ & \begin{bmatrix} X_2 & I_n \\ I_n & \frac{\pi}{2} I_n + \tau \mathcal{A} \end{bmatrix} \succeq 0. \end{aligned} \tag{5.5}$$

A solution (X_1, X_2, w_e) is optimal for (5.5) if and only if w_e is optimal for (5.1) when approximation (5.3) is applied [10]. Note that the objective function in (5.5) is a linear function of optimization variables X_1, X_2, and w_e.

This approach provides the optimal vector of edge weights $\boldsymbol{w}^*$ to minimize the performance loss when all the nodes are subject to a normal noise distribution. Next, we will present a robust optimization algorithm for the case where noise distribution is not necessarily normal.

5.2. Robust traffic restriction. In what follows, we consider the epidemic network with dynamics (3.1) when the input noise of subpopulation i is $\xi_i \sim \mathcal{N}(0, \sigma_i^2)$ for $i = 1, 2, \ldots, n$. We assume that $0 \le \sigma_i^2 \le 1$ and let $\sum_{i \in \mathcal{V}} \sigma_i^2 = n$. We then develop a new traffic control algorithm such that the highest performance loss with respect to the noise variance, σ_i, is minimized. In other words, this is a min-max problem which is cast as

$$\begin{aligned} \underset{w_e, \forall e \in \mathcal{E}}{\text{minimize}} \quad & \underset{\sigma_i, \forall i \in \mathcal{V}}{\text{maximize}} \ \rho_{\text{ss}} \\ \text{subject to} \quad & \sum_{i \in \mathcal{V}} \sigma_i^2 = n, \\ & \underline{w}_e \le w_e \le \overline{w}_e, \\ & \sum_{e \in \mathcal{E}} w_e = c, \\ & \mathcal{A} = \beta \sum_{e \in \mathcal{E}} w_e A_e + \beta \operatorname{diag}(A) - \delta I_n, \\ & -\frac{\pi}{2\tau} I_n \preceq \mathcal{A} \preceq -\epsilon I_n. \end{aligned} \tag{5.6}$$

$\sum_{i\in\mathcal{V}}\sigma_i^2 = n$ is a constraint on the sum of noise variance for all the agents, which allows for a nonuniform noise distribution between them. The rest of the constraints are the same as explained for problem (5.1). The solution to the inner optimization loop is

$$\begin{aligned} S = \underset{\sigma_i,\forall i\in\mathcal{V}}{\text{maximize}} \ & \rho_{\text{ss}} \\ \text{subject to} \ & \sum_{i\in\mathcal{V}}\sigma_i^2 = n, \end{aligned} \tag{5.7}$$

which allows for comparing network performance loss with different noise distribution scenarios and identifying the noise distribution that results in the highest performance loss among them. Using the performance definition in (4.3), the optimization problem (5.7) can be rewritten as

$$\begin{aligned} S = \underset{\sigma_i,\forall i\in\mathcal{V}}{\text{maximize}} \ & \sum_{i\in\mathcal{V}}\eta_i\sigma_i^2 \\ \text{subject to} \ & \sum_{i\in\mathcal{V}}\sigma_i^2 = n. \end{aligned} \tag{5.8}$$

Since the objective and constraint in problem (5.8) are linear functions of σ_i^2, the maximum performance loss occurs in the boundaries of $\sum_{i\in\mathcal{V}}\sigma_i^2 = n$, where for one subpopulation with highest centrality we have $\sigma_i^2 = n$, while for the rest of the subpopulations we have $\sigma_i^2 = 0$. We denote this case as an *extreme noise distribution* and present the solution, σ_i^*, to problems (5.7) and (5.8) as follows:

$$\sigma_i{}^* := \begin{cases} \sqrt{n} & \text{if } i = \text{argmax}_{j\in\mathcal{V}}\,\eta_j, \\ 0 & \text{otherwise.} \end{cases} \tag{5.9}$$

Using the node centrality measure found in Corollary 4.2 and employing (5.9) in the performance measure found in (4.2), the solution to problem (5.7) is equal to

$$\begin{aligned} S &= \max\left\{ s \,\middle|\, s = n\eta_i, i\in\mathcal{V} \right\} \\ &= \max\left\{ s \,\middle|\, s = -\frac{n}{2}\left[\mathcal{A}^{-1}\cos(\tau\mathcal{A})\left(I_n + \sin(\tau\mathcal{A})\right)^{-1}\right]_{ii}, i\in\mathcal{V} \right\}. \end{aligned} \tag{5.10}$$

Note that this solution is a nonconvex function of w_e, the optimization variable of problem (5.6). Therefore, its approximation found in (5.3) will be used.

Problem (5.6) can now be expressed in the following convex form:

$$\begin{aligned} \underset{\substack{X_1;X_2 \\ S;w_e,\forall e\in\mathcal{E}}}{\text{minimize}} \ & S \\ \text{subject to} \ & \underline{w}_e \le w_e \le \overline{w}_e, \\ & \sum_{e\in\mathcal{E}} w_e = c, \end{aligned}$$

$$
\begin{aligned}
&\mathcal{A} = \beta \sum_{e\in\mathcal{E}} w_e A_e + \beta \mathrm{diag}\,(A) - \delta I_n,\\
&-\frac{\pi}{2\tau} I_n \preceq \mathcal{A} \preceq -\epsilon I_n,\\
&S \geq \frac{n}{2}\left[-X_1 + \frac{4\tau}{\pi} X_2 - c_1\tau^2 \mathcal{A}\right]_{ii},\\
&\begin{bmatrix} X_1 & I_n \\ I_n & \mathcal{A} \end{bmatrix} \succeq 0,\\
&\begin{bmatrix} X_2 & I_n \\ I_n & \frac{\pi}{2} I_n + \tau\mathcal{A} \end{bmatrix} \succeq 0.
\end{aligned} \tag{5.11}
$$

The fifth constraint is the approximated version of (5.10) for any $i \in \mathcal{V}$ obtained by (5.3). This constraint should hold for all $i \in \mathcal{V}$, which results in obtaining the highest approximated performance loss by finding the first central node with respect to the epidemic-based centrality.

Remark 5.1. While the solution to optimization problem (5.5) depends on the performance measure of the entire network, the robust problem (5.11) incorporates the epidemic-based centrality of the most important node in the network to establish a policy that can potentially improve the entire network's robustness against extreme noise distributions. The node centrality index contains important network and epidemic information, i.e., transportation network structure as well as epidemic delays and rates. It therefore enables finding a criterion for ranking nodes based on not only their location in the transportation network but also the epidemic characteristics.

Remark 5.2. Let S_A be the solution to problem (5.7) obtained from epidemic-based centrality, and let S_B be the solution obtained from other centralities. The following lemma compares the optimal solutions of problem (5.7).

Lemma 5.3. *Consider epidemic network* (3.1) *over a weighted undirected graph* $\mathcal{G}$ *with adjacency matrix* $A = [a_{ij}] \in \mathbb{R}^{n\times n}$*, infection rate* β*, recovery rate* δ*, and time delay* $0 < \tau < \frac{-\pi}{2\lambda_1}$*. The solution obtained for problem* (5.7) *is suboptimal when using any centrality measure, except for epidemic-based centrality.*

Proof. The optimization problem (5.7) can be expressed as

$$
\begin{aligned}
S = \underset{\sigma_i, \forall i\in\mathcal{V}}{\text{maximize}} \quad & -\frac{1}{2}\,\mathrm{Tr}\left[BB^\top \mathcal{A}^{-1}\cos(\tau\mathcal{A})\,(I_n + \sin(\tau\mathcal{A}))^{-1}\right]\\
\text{subject to} \quad & \sum_{i\in\mathcal{V}} \sigma_i^2 = n.
\end{aligned} \tag{5.12}
$$

As found by (5.10), one approach for determining S is to rewrite ρ_{ss} using the definition of epidemic-based centrality, which yields $S_A = n\eta_k$, where k is the node with the highest epidemic-based centrality η_k.

Using any other centrality measure, such as degree, betweenness, or eigenvector, will result in having either the same node $j = k$ with the highest centrality, or a different node $j \in \mathcal{V} \setminus k$ as the most central node. In such cases, the performance loss can be expressed as $\rho_{ss} = \sum_{j\in\mathcal{V}} \eta_j \sigma_j^2 \leq n\eta_k$, which implies that S_B, the maximum value of ρ_{ss} obtained using any other centrality measure, will be less than or equal to S_A. ∎

Remark 5.4. In this section, we presented optimization problems that could also be solved using numerical optimization techniques, such as the interior-point method, which can be implemented using optimizers like fmincon in MATLAB, provided that an accurate initial point for the decision variables (i.e., network edge weights) is available. However, through approximating performance measures and convexifying the robust optimization problems in section 5, we gained insight into the significance of epidemic-based centrality in identifying an optimal traffic flow for epidemic containment. Although we can use numerical optimizers to solve (5.11), this would not provide clear intuition about the importance of epidemic-based centrality.

6. Simulation results. In this section, the theoretical results obtained in previous sections will be implemented on a core-periphery network and a network of the 15 busiest U.S. airports.

We use the following notation in the presented results:

- **Network A1**: The core-periphery network with no traffic restrictions.
- **Network A2**: The core-periphery network when the optimal traffic restriction is implemented.
- **Network A3**: The core-periphery network when the robust traffic restriction by epidemic centrality is implemented.
- **Network B1**: The U.S. airport network with no traffic restrictions.
- **Network B2**: The U.S. airport network when the optimal traffic restriction is implemented.
- **Network B3**: The U.S. airport network when the robust traffic restriction by epidemic-based centrality is implemented.
- **Network B4**: The U.S. airport network when the robust traffic restriction by degree centrality is implemented.

It is worth mentioning that for both the core-periphery network and the network of 15 busiest U.S. airports, we utilized fmincon with LMI constraints to identify the optimal network. When an appropriate initial guess for edge weights was provided, we obtained the same results as with convex optimization.

6.1. Core-periphery network. Consider the network presented in Figure 4(a) with three connected star graphs consisting of $|\mathcal{V}_A| = 20$ nodes and $|\mathcal{E}_A| = 19$ weighted edges. The edge weights are randomly associated with a value in $[0.2, 1]$, which is specified by the color of the edges. Nodes are ranked based on their epidemic-based centrality index, η_i, which is reflected through the size of their indicating circles. We denote the defined network by Network A1 (see Figure 4(a)). In this network, when local social distancing is followed, i.e., $a_{ii} = 0$ for $i \in \mathcal{V}_A$, the eigenvalues of the adjacency matrix are arranged as $u_i \in [-2.52, 2.52]$, resulting in a stability range of $\tau \in [0, 17.39]$ days for the time delay. On the other hand, if none of the subpopulations follows local social distancing, i.e., $a_{ii} = 1$ for $i \in \mathcal{V}_A$, the stability range of time delay will extend to 22.04 days. Assume that all the subpopulations are experiencing 17 days of delay, which will result in a stable network regardless of the status of local social distancing. A combination of multiple star graphs is a good candidate for an epidemic network, as in reality some of the subpopulations are the hubs. while the others connect to the rest of the subpopulations through these hubs. In this network, nodes 1, 2, and 15 are the hubs.

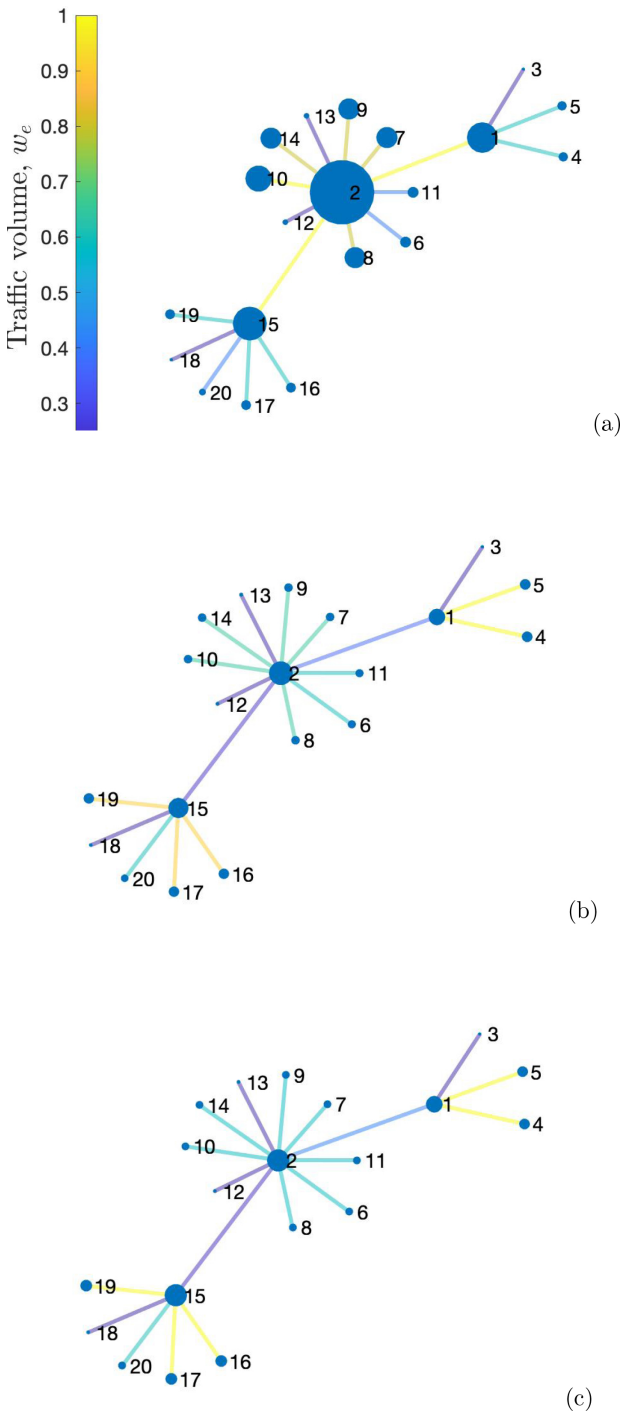

Figure 4. (a) *Network A1 with* $\mathcal{R}_{0M} = 0.806$. (b) *Network A2 with* $\mathcal{R}_{0M} = 0.607$. (c) *Network A3 with* $\mathcal{R}_{0M} = 0.603$. *All the networks are following local social distancing and experiencing* $\tau = 17$ *days of time delay. The nodes are ranked based on their epidemic-based centrality index,* η_i*, which is reflected through the size of their indicating circle. The interconnections are ranked by their corresponding traffic volume, which is specified by the color of the edges.*

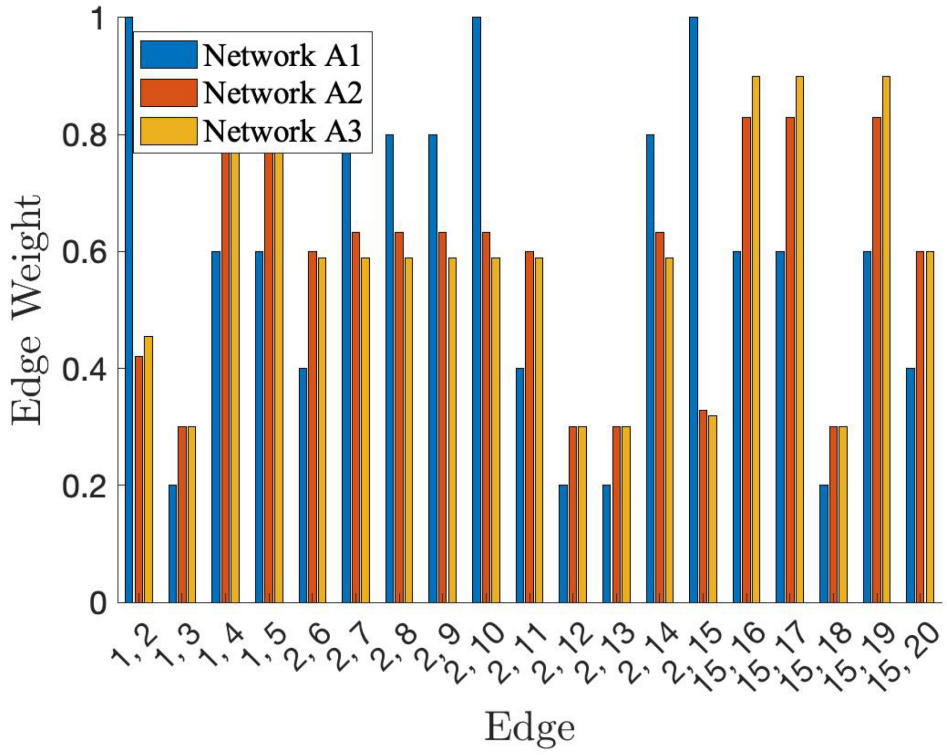

Figure 5. *Edge weight (traffic volume) comparison between Networks A1–A3 with $\tau = 17$ days and complete local social distancing for all $i \in \mathcal{V}_A$.*

Note that Figures 4–8 are obtained based on Network A1 with dynamics (3.1) when a complete local social distancing is followed. When applying the convex optimization method (5.5) with c equal to the overall traffic volume, the network structure changes into Network A2, shown in Figure 4(b). The implemented traffic optimizer has successfully reduced the network performance loss due to exogenous noises by reducing the centrality index of nodes that are highly contributing to disease propagation. Figure 4(c) presents Network A3, which is the result of implementing robust optimization approach (5.11) for the same value of c on Network A1 with dynamics (3.1) and complete local social distancing. The robust optimization is designed to consider the worst-case scenario, where the extreme noise distribution amplifies the effect of hub node 2 with the highest centrality. Hence, the robust optimizer is more conservative in manipulating the traffic volumes and reducing the centrality of hubs. More detailed comparisons of optimal and robust networks are presented in the following figures.

The comparison between edge weights and node centrality indices of Networks A1–A3 in Figure 4 can be found in the bar diagrams of Figures 5 and 6, respectively.

Figure 7(a) presents the logarithmic performance measure of Networks A1–A3 with respect to the desired traffic volume, c, when the network is experiencing a uniform noise distribution. The results indicate that with the same noise distribution, the nondelayed versions of Networks A1–A3 maintain a higher performance compared to the delayed networks. This result can

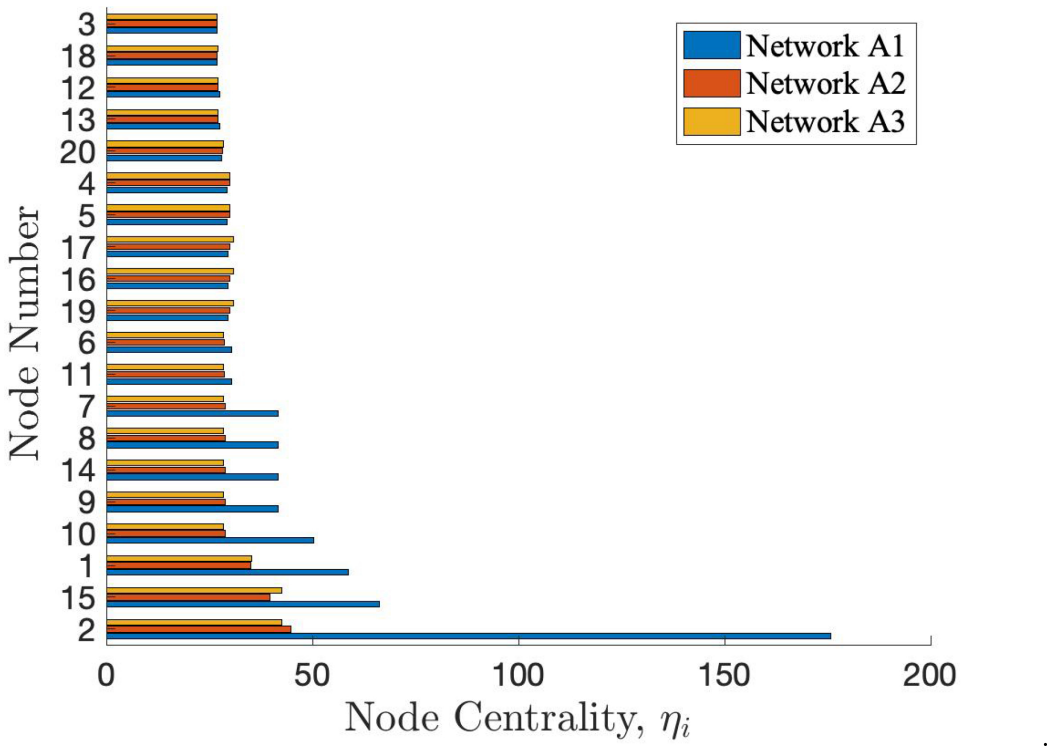

Figure 6. *Epidemic-based centrality index comparison between Networks A1–A3 with $\tau = 17$ days and complete local social distancing for all $i \in \mathcal{V}_A$.*

be verified by (4.2). As the desired traffic volume increases to its nominal value (e.g., traffic volume with no restrictions), the performance loss will monotonically increase for both delayed and nondelayed networks. When reaching the nominal traffic volume, the traffic restriction on one edge has to be compensated by increasing the traffic capacity on another, less important edge, which results in a significant loss of performance. Given a desired traffic volume, both the optimal and robust traffic controllers will aim to decrease the performance loss, while the optimal approach results in a slightly better performance due to its less conservative weight distribution algorithm.

To emphasize the importance of considering worst cases while determining the intensity of traffic restriction, a comparison between the maximum performance measure of both optimization methods is presented in Figure 7(b). In the case of extreme noise distribution, Network A3 is expected to experience less performance loss, as it is specifically designed to be robust against extreme noise distributions.

As shown in Figure 8, the performance loss of networks in Figure 4 increases monotonically as the time delay increases.

The effect of time delay on the epidemic evolution of Network A1 with dynamics (2.7) when local social distancing is followed ($a_{ii} = 0$ for $i = 1, 2, \ldots, n$) is illustrated in Figure 9. When the network is experiencing a time delay, it might undergo multiple infection fluctuations

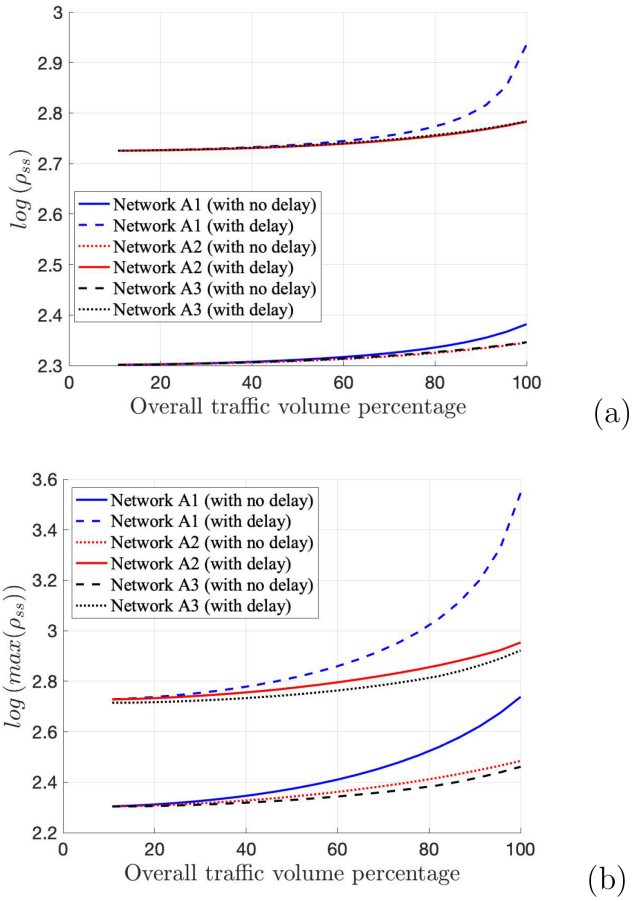

Figure 7. (a) *Performance loss comparison between nondelayed and delayed ($\tau = 17$ days) versions of Networks A1–A3 in the case of uniform noise distribution and complete local social distancing for all $i \in \mathcal{V}_A$.* (b) *Performance loss comparison between nondelayed and delayed ($\tau = 17$ days) versions of Networks A1–A3 in the case of extreme noise distribution and complete local social distancing for all $i \in \mathcal{V}_A$.*

before reaching a steady state, while a network with no time delay will experience a smooth transition. As the intrinsic time delays increase, the network will experience a more extreme epidemic peak with multiple pulses. The time delay also shows a correlation with the onset of the epidemic peak, which is a decisive factor in designing the proper traffic restriction policies. Note that the selected reproduction number is set significantly high in order to emphasize the effect of time delay. If an infection with a reproduction number of $\mathcal{R}_{0M} = 4.7$ spreads within one subpopulation at time t, it is expected to directly infect approximately 4.7 other subpopulations at time $t + \tau$.

The average infection size of the networks in Figure 4(a)–(c), where 10% of the network is initially infectious and there is no local social distancing in subpopulations, i.e., $a_{ii} = 1$ for all $i \in \mathcal{V}$, is shown in Figure 10. Unlike Network A1 with no delay, which shows no fluctuations, the delayed version of Network A1 is experiencing multiple pulses. When

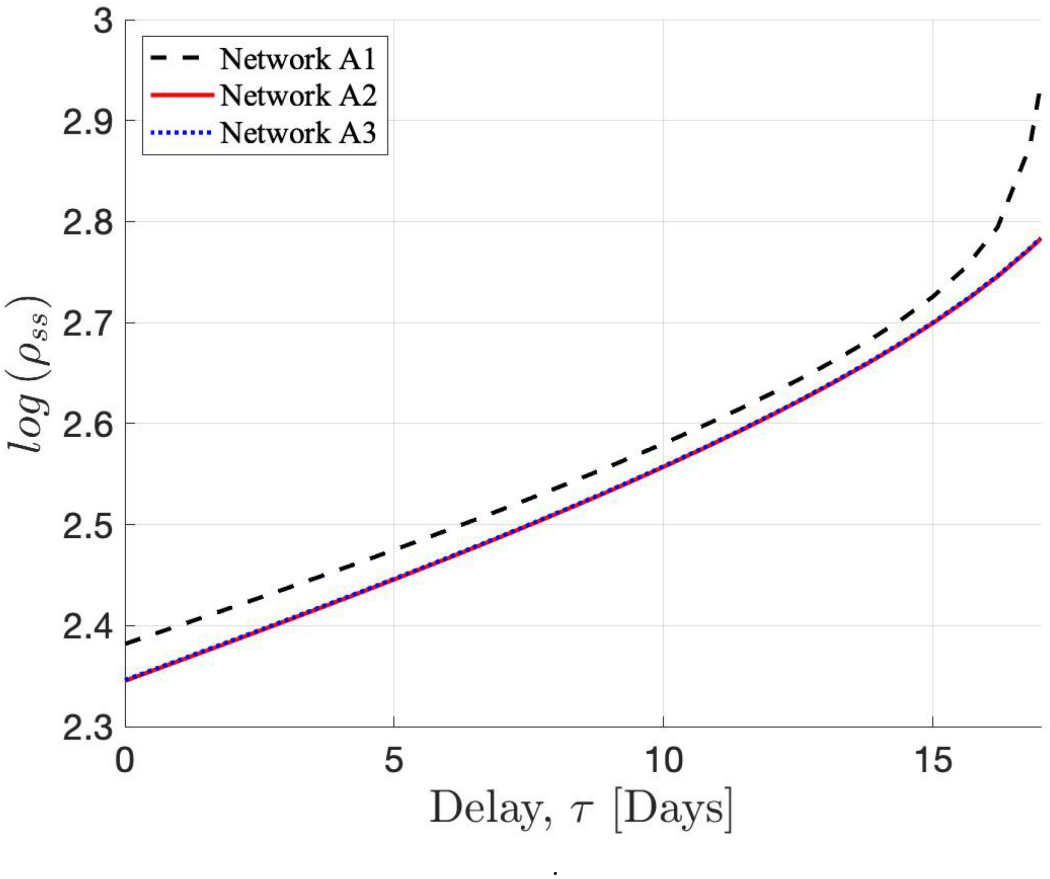

Figure 8. *Logarithmic performance measure of Networks A1–A3 with respect to time delay when complete local social distancing is followed by all* $i \in \mathcal{V}_A$.

applying the proposed traffic restriction policies on this network, which results in Networks A2 and A3, the epidemic will eventually die out after about 500 days, while in Network A1 it will take longer for the infection to become extinct.

More details on performance improvement through optimal and robust traffic controllers are presented in Table 1. Case 1 indicates a uniform noise distribution, i.e., $\sigma_i = 1$ for $i = 1, 2, \ldots, n$. Case 2 indicates an extreme noise distribution (see (5.9)).

Remark 6.1. The delayed SIS model introduced in this paper is potentially relevant to the spread of COVID-19 or other diseases with similar transmission characteristics, for which a clear immunity is not guaranteed. In particular, the 11-day delay we incorporated in simulating the network of the 15 busiest U.S. airports could represent the latent period of the disease, during which the infected individual may not show symptoms but may still be capable of transmitting the disease to others. However, it is important to note that our model has several limitations and simplifying assumptions. For example, we did not consider the effects of interventions such as vaccination or contact tracing, which can greatly impact the dynamics of disease transmission.

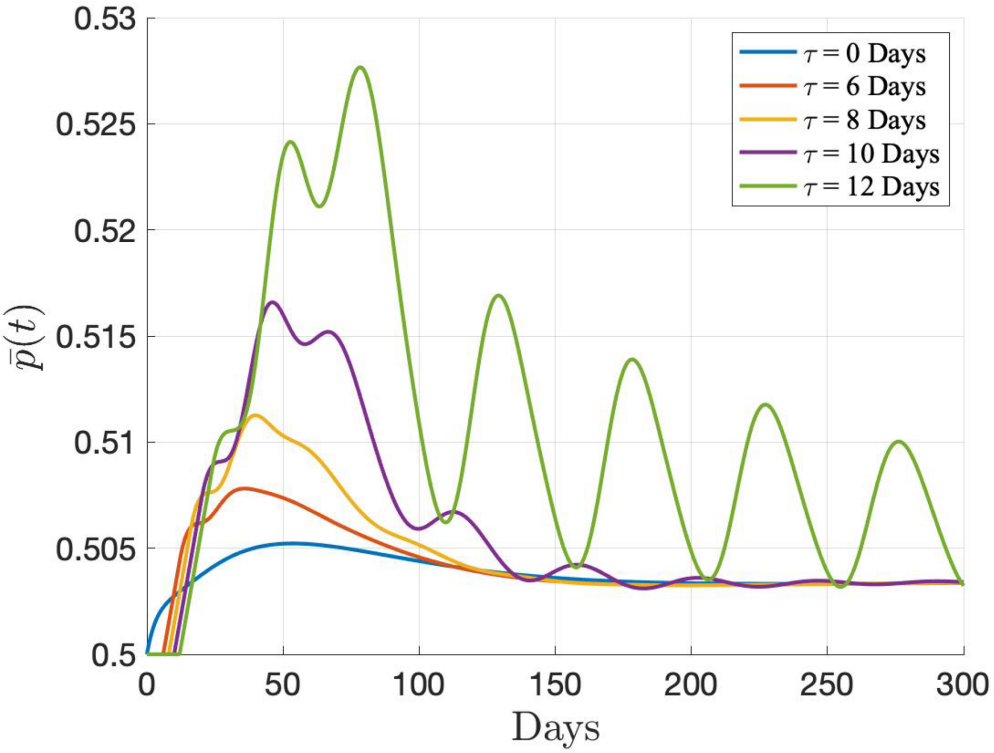

Figure 9. *Average infection size, $\bar{p}(t) = \frac{1}{n}\sum_{i\in\mathcal{V}} p_i(t)$, of Network A1 with nonlinear dynamics (2.7) when complete local social distancing is followed by all $i \in \mathcal{V}_A$. Fifty percent of the metapopulation is initially infectious and $\mathcal{R}_{0M} = 4.7$.*

6.2. Network of the 15 busiest U.S. airports. Air transportation plays an important role in introducing a new disease to a metapopulation and spreading infection within its subpopulations. In this study, a group of the busiest U.S. airports is selected as the representation of an epidemic network. The original network shown in Figure 11(a) consists of $|\mathcal{V}_B| = 15$ airports connected by $|\mathcal{E}_B| = 104$ weighted edges, which represent air traffic flow between the airports. In this network, when local social distancing is followed, i.e., $a_{ii} = 0$ for $i \in \mathcal{V}_B$, the eigenvalues of the adjacency matrix are arranged as $u_i \in [-1.58, 6.64]$, resulting in a stability range of $\tau \in [0, 11.30]$ days for the time delay. On the other hand, if none of the subpopulations follows local social distancing, i.e., $a_{ii} = 1$ for $i \in \mathcal{V}_B$, the eigenvalues of the adjacency matrix are arranged as $u_i \in [-0.58, 7.64]$, and the stability range of time delay will extend to 12.71 days. We assume that the airports are experiencing 11 days of delay, which will result in a stable network regardless of the status of local social distancing. In Figure 11(a), the airports are ranked based on their epidemic-based centrality index, η_i, which is indicated by the size of the circles located in the geographical position of each airport. The interconnection between every pair of nodes is ranked based on the air traffic volume between them, which is specified by the color of the links. The U.S. air traffic data used in this study can be found in [46].

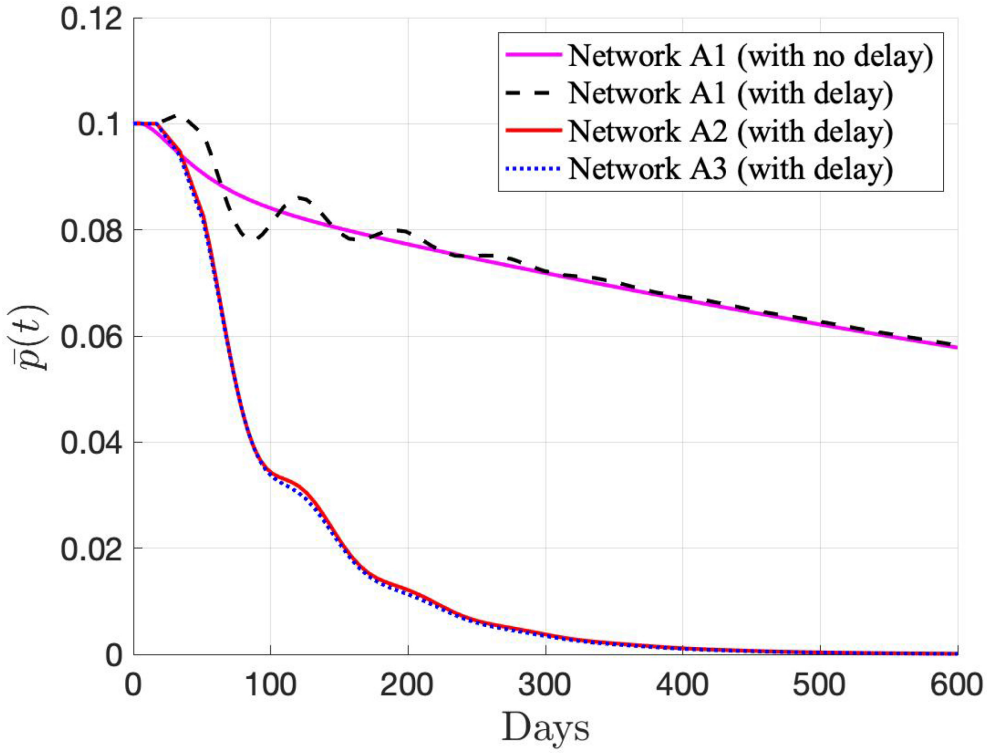

Figure 10. *Average infection size of Network A1 with no delay and Networks A1–A3 with $\tau = 17$ days, $\mathcal{R}_{0M} = 0.98$, and initial infection of 10%. All the networks are following dynamics (2.9) with no effective local social distancing for all $i \in \mathcal{V}_A$.*

Table 1

The values and percentages of performance enhancement for Networks A1–A3 (Figure 4) and Network A4.

	Case 1	Case 2
Network A1 (Figure 4(a))	862 (0%)	3514 (0%)
Network A2 (Figure 4(b))	606 (+29%)	898 (+74%)
Network A3 (Figure 4(c))	607 (+29%)	835 (+76%)

We assume that one of the subpopulations is initially infected. The infectious population of its neighbors will gradually increase due to their connection through air transportation. Applying the proposed optimal traffic control method (5.5) on this network results in the network of Figure 11(b) with a lower range of centrality for all the nodes. Furthermore, implementing the robust optimization approach (5.11) on Network B1 will change the network structure to that in Figure 11(c) with smaller centrality values. Note that the robust controller has considered an extreme noise distribution and has therefore adjusted the traffic volume around highly centered nodes to reduce their centrality index significantly.

Figure 12 represents the average infection size of Network B1 with a complete local social distancing and $\tau = 12$ days of delay. The dashed blue and solid black lines display, respectively,

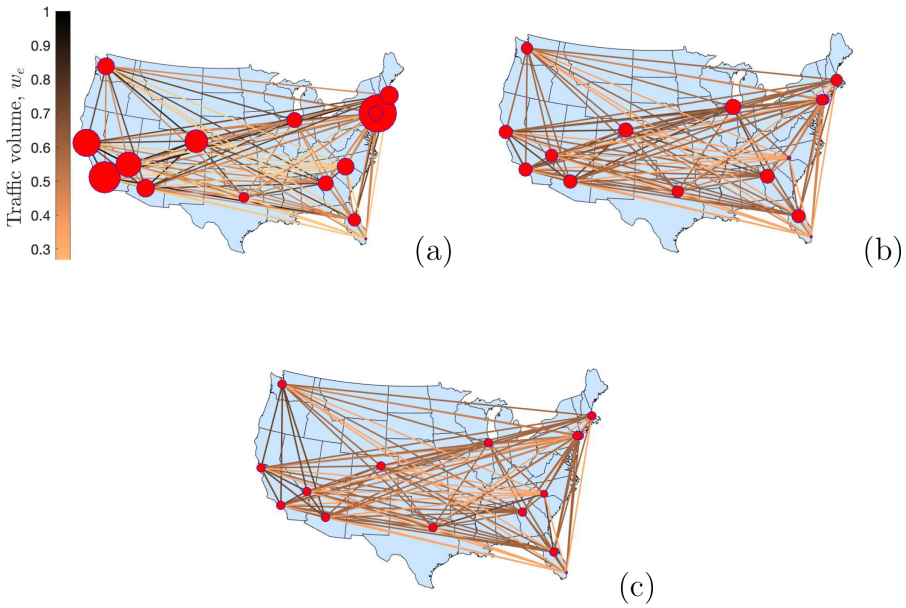

Figure 11. (a) *Network B1 with* $\mathcal{R}_{0M} = 0.892$. (b) *Network B2 with* $\mathcal{R}_{0M} = 0.875$. (c) *Network B3 with* $\mathcal{R}_{0M} = 0.868$. *All the subpopulations are following local social distancing and experiencing* $\tau = 11$ *days of time delay. Each hub is ranked based on its epidemic-based centrality index,* η_i*, which is reflected through the size of its indicating circle. The interconnections are ranked by their corresponding traffic volume, which is specified by the color of the edges.*

$\bar{p}(t)$ for dynamics (2.9) without any noise, and dynamics (3.1) with exogenous noise input of zero mean and $\sigma_i^2 = 0.01$ for all $i \in \mathcal{V}_B$. The solid red line displays the average of $\bar{p}(t)$ of the noisy network over 1000 simulations with different random noises, and the red shaded area represents the standard deviation of simulations. This figure illustrates the impact of both small shocks and time delays on the occurrence of successive waves of infection.

Figure 13 shows the infection size of Network B1 with nonlinear dynamics (2.7) and different time delays when 5050% of the metapopulation is initially infectious. All the nodes are following local social distancing, and $\mathcal{R}_{0M} = 2.3$. When there is no delay ($\tau = 0$) or only a small delay, the epidemic dynamics of the network do not show fluctuations. However, as the delay increases, epidemic pulses start to appear. For instance, a delay of 12 days leads to an approximately 2% increase in the average infection size within the first 30 days of the epidemic, which corresponds to a considerable number of individuals within the U.S. population. As mentioned earlier, the system remains stable for delays of up to 11.30 days. Therefore, when there is a 12-day delay, the average infection size will continue to increase without bounds as time passes.

Consider Networks B1–B4 with dynamics described as in (3.1) and a time delay of $\tau = 11$ days. To determine the average infection size of Networks B1–B4 when only the epidemic-based central node, New York, experiences a small shock, we conducted 1000 simulations with different random noises. The results are presented in Figure 14, where the solid lines represent the average of $\bar{p}(t)$, and the shaded area represents the standard deviation of the

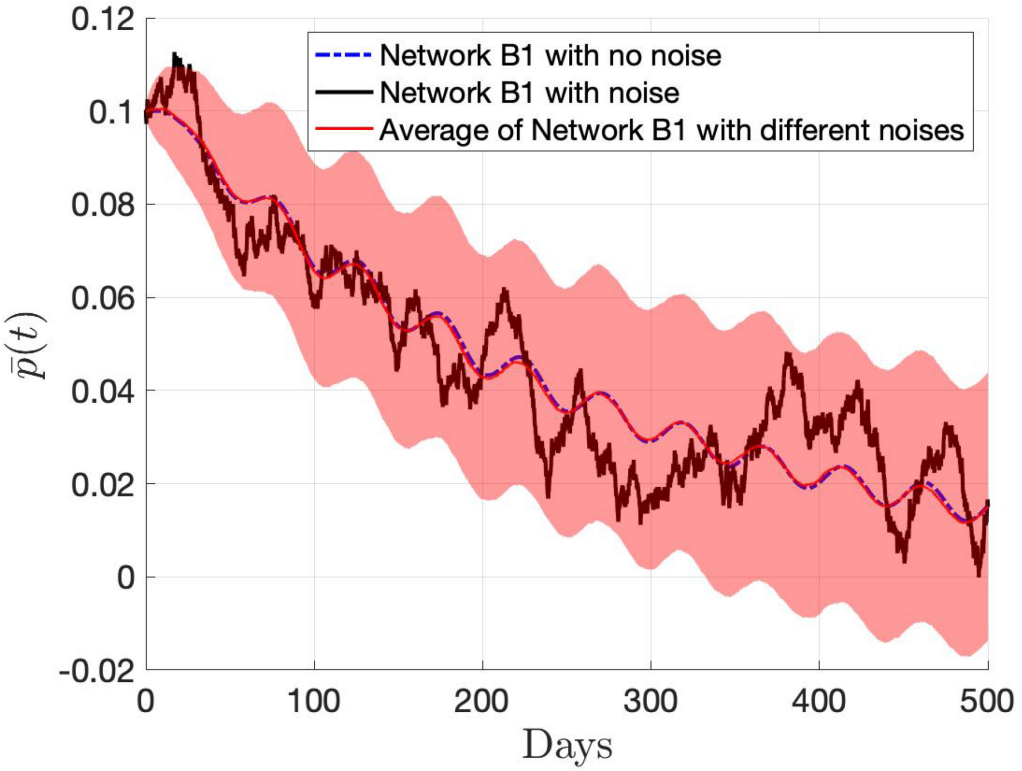

Figure 12. *Average infection size of Network B1 with no noise (dashed blue), and a random noise (solid black) over time. The solid red line represents the average of* $\bar{p}(t)$ *over* 1000 *simulations with different random noises. The red shaded area represents the standard deviation of the simulations. In all the simulations the network follows linear dynamics* (3.1) *with complete local social distancing. Time delay is* $\tau = 12$ *days,* $\mathcal{R}_{0M} = 0.96$*, and initial infection is* 10% .

simulations. It was found that Network B4, which used the degree centrality to rank the nodes and optimize the traffic volume to minimize highest performance loss, was less effective in reducing the average infection size over time. This is in contrast to the other networks, including Network B1 with no traffic restrictions, and Networks B2–B3 with traffic restrictions based on epidemic factors and delays.

Figure 15 shows the logarithmic performance loss of Networks B1–B3 with respect to time delay. As expected, the network experiences a lower performance loss when applying traffic restriction methods. Figure 16 displays the normalized epidemic-based centrality index of nodes for Networks B1–B3, as well as the normalized degree centrality index of nodes for Networks B1 and B4. There is a significant difference in the epidemic-based centrality index of nodes between Networks B1, B2, and B3. When comparing the implementation of robust control using epidemic-based centrality (Network B3) and degree centrality (Network B4), it is found that the former isolates the epidemic-based central airport, New York, to a greater extent than the latter; Los Angeles is not the most isolated airport in Network B4.

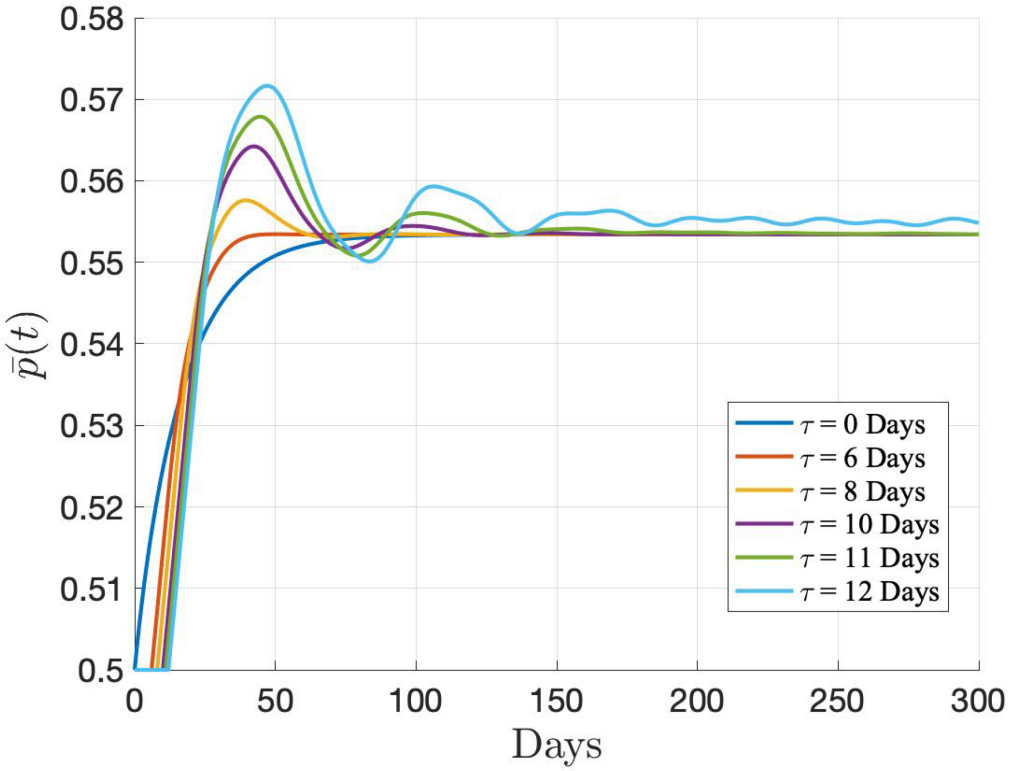

Figure 13. *Average infection size of Network B1 with nonlinear dynamics (2.7) and complete local social distancing for different time delays. Fifty percent of the metapopulation is initially infectious, and* $\mathcal{R}_{0M} = 2.3$.

The epidemic-based centrality difference between two nodes in the network, Atlanta and Chicago, with respect to basic reproduction number, is shown in Figure 17. When $\tau =$ 11 days, one interlacing between the selected nodes is observed. In other words, as the disease progresses and $\mathcal{R}_{0M}$ increases slowly enough over time, Atlanta becomes a more central subpopulation compared to Chicago, requiring more restrictive traffic control measures.

Furthermore, the detailed results of the performance improvement through optimal and robust epidemic controls are represented in Table 2 for Case 1 with uniform noise distribution, i.e., $\sigma_i = 1$ for $i = 1, \ldots, n$, and for Case 2 with extreme noise distribution (see (5.9)).

Table 3 presents a comparison between the top three central nodes based on the epidemic-based centrality defined in Corollary 4.2, degree centrality, and eigenvector centrality when $\tau = 11$ days. While degree and eigenvector centralities identify the same two nodes as most central ones, two of the three nodes based on epidemic-based centrality (4.1) are not captured by other centralities, due to its fundamental differences described in Remark 5.1. However, according to Theorem 4.4, when $\tau \to 0$, the result of epidemic-based centrality, $\mathcal{I}_e$, is expected to converge to that of local centrality, $\mathcal{I}_o$, as $\frac{\beta}{\delta} \to 0^+$. On the other hand, when $\tau \to 0$, the output of epidemic-based centrality, $\mathcal{I}_e$, will converge to that of eigenvector centrality, $\mathcal{I}_{ev}$, as $\frac{\beta}{\delta} \to \frac{1}{u_n}^-$; see Theorem 4.5. Table 4 presents the top four ranking results for different ranges of $\mathcal{R}_{0M}$ when $\tau \to 0$ and $a_{ii} \in [0, 1]$ for all $i \in \mathcal{V}$. When only the top central nodes

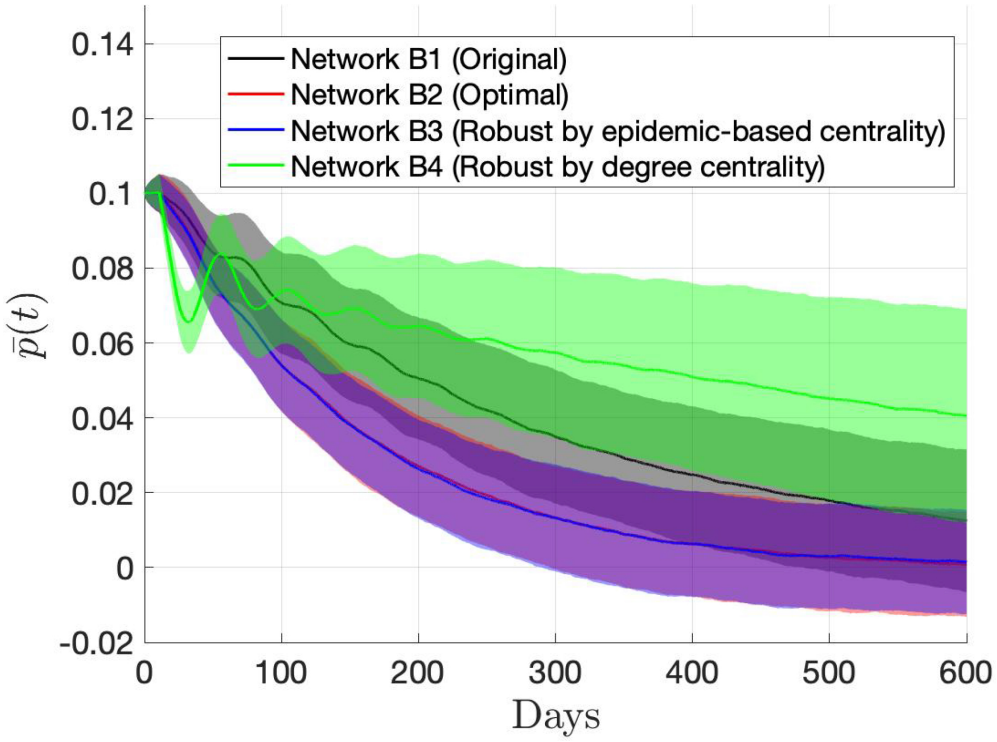

Figure 14. *Average of $\bar{p}(t)$ for Networks B1–B4 with $\tau = 11$ days, $\mathcal{R}_{0M} = 0.97$, and initial infection of 10%. All the networks follow the linear dynamics (3.1) with no effective local social distancing for all $i \in \mathcal{V}_B$. Results are obtained over 1000 simulations with different random noises on New York, the most central node according to epidemic-based centrality. The solid lines represent the average of $\bar{p}(t)$, while the shaded area represents the standard deviation of the simulations.*

are considered in the decision-making process, the rankings for $\mathcal{R}_{0M} \to 0^+$ and $\mathcal{R}_{0M} \to 1^-$ indicate that the effect of epidemic properties on the results is negligible. In such cases, a node's location in the network will determine its impact on the spread of disease. On the other hand, for $0.06 < \mathcal{R}_{0M} < 0.92$, the epidemic properties of disease will also contribute to the rankings provided by epidemic-based centrality, which leads to a different output.

7. Discussion. In this study, the linear SIS dynamics of an epidemic network subject to time delay and small shocks has been investigated. The network robustness against small shocks to its subpopulations is then analyzed using an $\mathcal{H}_2$-based metric. A customized epidemic-based node centrality is presented to rank the nodes based on their effect on the network performance while they are exposed to an external node-level shock. The introduced epidemic-based centrality is a function of adjacency matrix, epidemic rates, and time delay, which enables adaptive identification of central nodes as the disease progresses within the network. The performance measure and epidemic-based centrality index are then employed to develop optimal and robust traffic restriction methods, respectively. The objective is to improve network performance in the presence of time delay and external shocks, which are

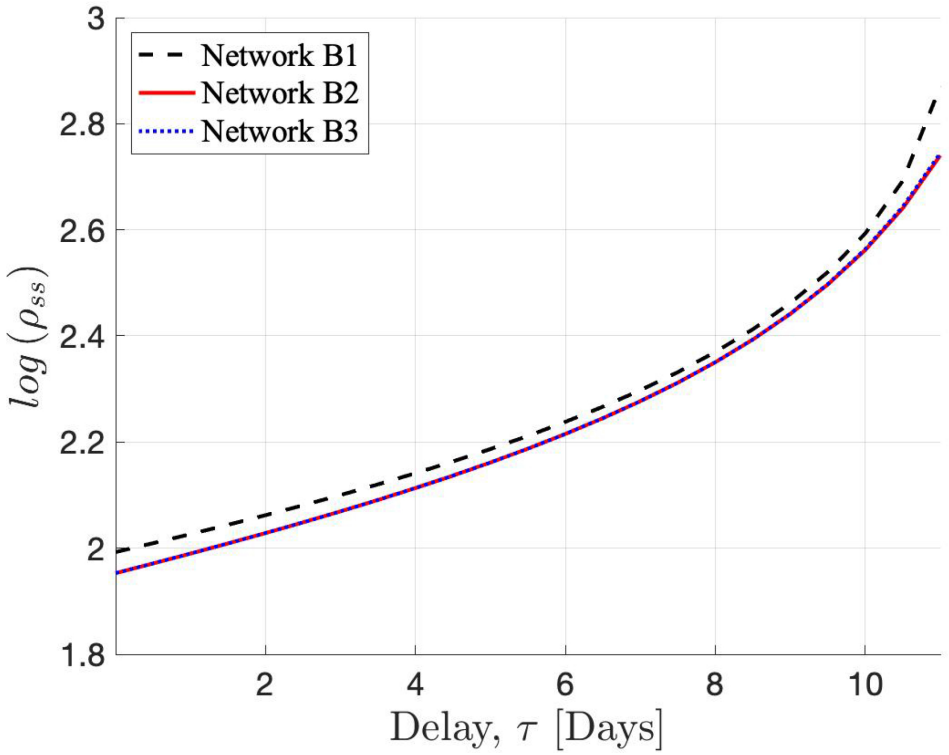

Figure 15. *Logarithmic performance measure of Networks B1–B3 with respect to time delay when complete local social distancing is followed by all $i \in \mathcal{V}_B$.*

modeled by additive Gaussian white noise input. The proposed methods are designed based on convexifying the original optimization problem to guarantee a global solution. The implementation of the proposed traffic restriction methods on a core-periphery network and a network of busiest U.S. airports indicates significant performance improvement along with mitigating successive waves of infection. Future research could expand on our model by incorporating existing epidemic datasets and considering the effects of interventions, such as vaccination, testing, and contact tracing.

7.1. Supplemental notes. The following animations are provided as supplementary material to help further clarify some of the notions presented in this study.

• This video (M150776_01.mov [local/web 22.0 MB]) shows the airport rankings of Network B1 for different values of $\mathcal{R}_{0M} \in (0,1)$ (2.10) when $\tau \to 0^+$. The rankings are obtained using epidemic-based centrality (4.1) for the network of the 15 busiest U.S. airports with dynamics (2.9). Each airport is indicated by its International Air Transport Association (IATA) code (a unique three-letter code), and its location is initially shown on the map. The size of the red circles is correlated with the epidemic-based centrality index of each airport, which is changing as $\mathcal{R}_{0M}$ increases. The colored links are indicators of normalized air traffic flow w_e between the airports. As proposed by Theorems 4.4 and (4.5), and also indicated in Table 4, the rankings provided by epidemic-based centrality slide between the rankings based on local

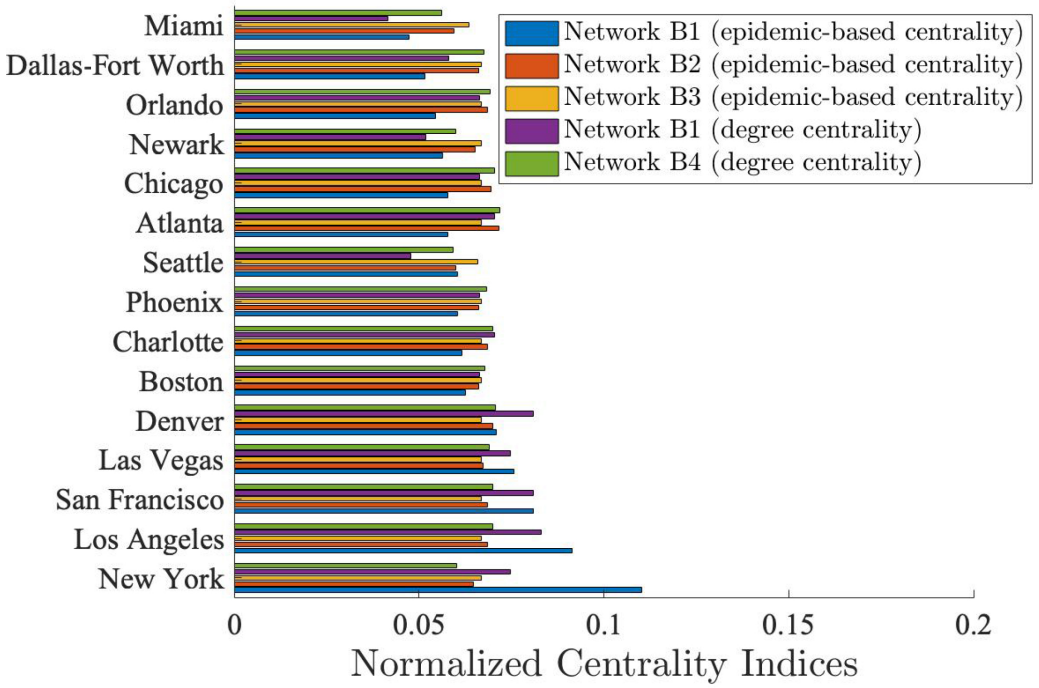

Figure 16. *Normalized epidemic-based and normalized degree centrality comparison between Networks B1–B4 with $\tau = 11$ days. All the networks follow the linear dynamics (3.1) with complete local social distancing.*

and eigenvector centralities; for $\mathcal{R}_{0M} \to 0^+$ we have $\mathcal{I}_e = \mathcal{I}_o$, and for $\mathcal{R}_{0M} \to 1^-$ we have $\mathcal{I}_e = \mathcal{I}_{ev}$. As the network reproduction number increases from near zero values, the less central airports begin to interlace (compare the rankings for $\mathcal{R}_{0M} \to 0^+$ and $\mathcal{R}_{0M} = 0.06$), while for higher reproduction numbers, interlacing happens in most central airports as well (compare the rankings for $\mathcal{R}_{0M} = 0.5$ and $\mathcal{R}_{0M} = 0.92$). As $\mathcal{R}_{0M}$ reaches its upper limit, the top-ranked airports no longer interlace (compare the rankings for $\mathcal{R}_{0M} = 0.92$ and $\mathcal{R}_{0M} \to 1^-$).

• This video (M150776_02.mov [local/web 10.5 MB]) presents the airport rankings for Network B1 with different values of time delay when its reproduction number is near zero. The rankings are obtained using epidemic-based centrality (4.1) for the network of the 15 busiest U.S. airports with dynamics (2.9). Each airport is indicated by its International Air Transport Association (IATA) code (a unique three-letter code), and its location is initially shown on the map. The size of the red circles is correlated with the epidemic-based centrality index of each airport, which is changing as $\mathcal{R}_{0M}$ increases. The colored links are indicators of normalized air traffic flow w_e between the airports. As proposed by Theorem 4.4, for time delays in $0 < \tau < \frac{z_1}{\delta}$, the output of local centrality o_i defined in (4.7) converges to that of epidemic-based centrality eta_i (4.1). On the other hand, when $\tau = \frac{z_1}{\delta}$, a completely different ranking will be provided by epidemic-based centrality, which is identical to that found by local centrality l_i (4.8). As time delay increases in its feasible range $\frac{z_1}{\delta} < \tau < \frac{\pi}{2\delta}$, the airports that were identified as less central for $0 < \tau < \frac{z_1}{\delta}$ turn into the most central ones, leading to an entirely reversed ranking result. The sudden and discrete variation of rankings with respect

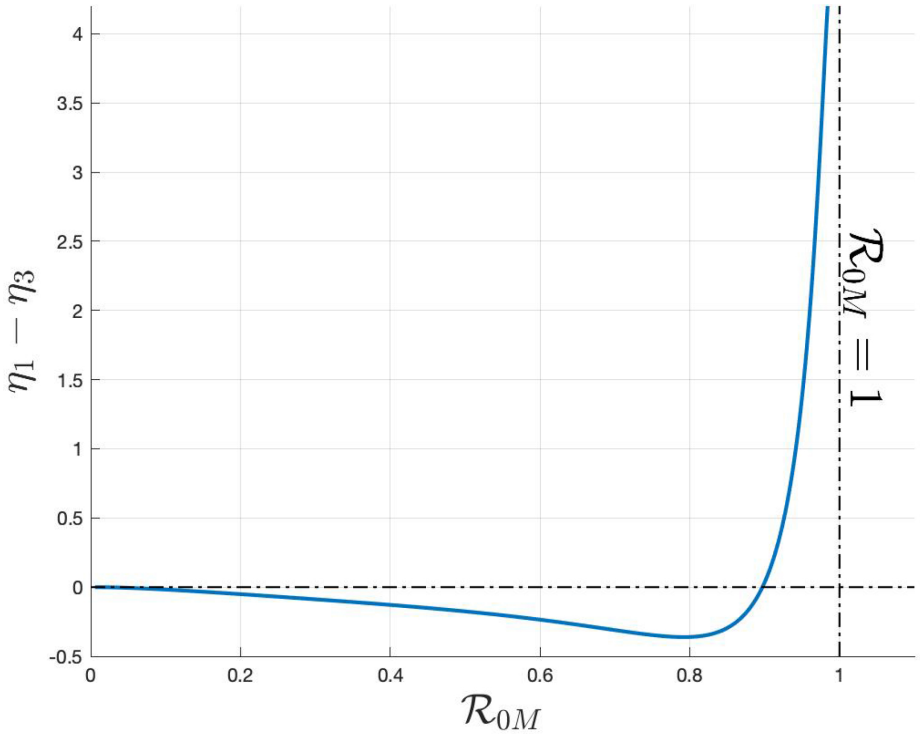

Figure 17. *Epidemic-based centrality difference between nodes* 1 *(Atlanta) and* 3 *(Chicago) of Network B*1 *with linear dynamics* (3.1) *and complete local social distancing versus network basic reproduction number* $\mathcal{R}_{0M}$ *for* $\tau = 11$ *days. The epidemic-based centrality of the two nodes interlaces once.*

Table 2

*The values and percentages of performance enhancement for Networks B*1*–B*3 *(Figure* 11*).*

	Case 1	Case 2
Network B1 (Figure 11(a))	741 (0%)	1227 (0%)
Network B2 (Figure 11(b))	549 (+25%)	590 (+51%)
Network B3 (Figure 11(c))	554 (+25%)	549 (+55%)

Table 3

Top three hubs based on different centralities when $\tau = 11$ *days.*

Epidemic-based centrality (4.1)	**Degree centrality**	**Eigenvector centrality**
New York	Los Angeles	Los Angeles
Los Angeles	Denver	Denver
San Francisco	Atlanta	Charlotte

to time delay indicates the importance of employing customized centrality indices, such as proposed epidemic-based centrality, which are capable of incorporating different factors of an epidemic disease into the decision-making process.

Table 4

Top four airport rankings by epidemic-based centrality for different values of $\mathcal{R}_{0M}$ when $\tau \to 0$.

Ranking	$0 < \mathcal{R}_{0M} \leq 0.06$	$\mathcal{R}_{0M} = 0.5$	$0.92 \leq \mathcal{R}_{0M} < 1$
1	Las Vegas	San Francisco	San Francisco
2	San Francisco	Las Vegas	Denver
3	Denver	Denver	Las Vegas
4	Miami	Phoenix	Los Angeles

REFERENCES

[1] D. Acemoglu, A. Ozdaglar, and A. Tahbaz-Salehi, *Networks, Shocks, and Systemic Risk*, Technical report, National Bureau of Economic Research, 2015.

[2] M. Aguiar, J. B. Van-Dierdonck, J. Mar, N. Cusimano, D. Knopoff, V. Anam, and N. Stollenwerk, *Critical fluctuations in epidemic models explain COVID-19 post-lockdown dynamics*, Sci. Rep., 11 (2021), pp. 1–12.

[3] R. M. Anderson and R. M. May, *Infectious Diseases of Humans: Dynamics and Control*, Oxford University Press, 1992.

[4] D. Antona, D. Lévy-Bruhl, C. Baudon, F. Freymuth, M. Lamy, C. Maine, D. Floret, and I. P. Du Chatelet, *Measles elimination efforts and* 2008–2011 *outbreak, France*, Emerg. Infect. Dis., 19 (2013), pp. 357–364.

[5] N. T. Bailey, *Macro-modelling and prediction of epidemic spread at community level*, Math. Model., 7 (1986), pp. 689–717.

[6] B. Bamieh, M. R. Jovanovic, P. Mitra, and S. Patterson, *Coherence in large-scale networks: Dimension-dependent limitations of local feedback*, IEEE Trans. Automat. Control, 57 (2012), pp. 2235–2249, https://doi.org/10.1109/TAC.2012.2202052.

[7] A. Banerjee, A. G. Chandrasekhar, E. Duflo, and M. O. Jackson, *The diffusion of microfinance*, Science, 341 (2013), 1236498.

[8] A. Banerjee, A. G. Chandrasekhar, E. Duflo, and M. O. Jackson, *Gossip: Identifying Central Individuals in a Social Network*, Technical report, National Bureau of Economic Research, 2014.

[9] M. Benzi and C. Klymko, *On the limiting behavior of parameter-dependent network centrality measures*, SIAM J. Matrix Anal. Appl., 36 (2015), pp. 686–706, https://doi.org/10.1137/130950550.

[10] S. Boyd and L. Vandenberghe, *Convex Optimization*, Cambridge University Press, 2004.

[11] R. Carli, G. Cavone, N. Epicoco, P. Scarabaggio, and M. Dotoli, *Model predictive control to mitigate the COVID-*19 *outbreak in a multi-region scenario*, Annu. Rev. Control, 50 (2020), pp. 373–393.

[12] E. Cator and P. Van Mieghem, *Second-order mean-field susceptible-infected-susceptible epidemic threshold*, Phys. Rev. E, 85 (2012), 056111.

[13] A. Darabi and M. Siami, *Centrality in epidemic networks with time-delay: A decision-support framework for epidemic containment*, in Proceedings of the 2021 American Control Conference (ACC), IEEE, 2021, pp. 3062–3067.

[14] A. Darabi and M. Siami, *Stability and robustness analysis of epidemic networks with multiple time-delays*, in Proceedings of the 2022 American Control Conference (ACC), IEEE, 2022, pp. 3668–3674.

[15] Y. Ding, Z. Jin, and J. Lou, *An SEIS epidemic model on scale-free network with recruitment and death*, J. Nonlinear Funct. Anal., 2015 (2015), 12.

[16] J. Doyle, K. Glover, P. Khargonekar, and B. Francis, *State-space solutions to standard $\mathcal{H}_2$ and $\mathcal{H}_\infty$ control problems*, IEEE Trans. Automat. Control, 34 (1989), pp. 831–847.

[17] A. d'Onofrio, *A note on the global behaviour of the network-based SIS epidemic model*, Nonlinear Anal. Real World Appl., 9 (2008), pp. 1567–1572.

[18] C. Enyioha, A. Jadbabaie, V. Preciado, and G. Pappas, *Distributed resource allocation for control of spreading processes*, in Proceedings of the 2015 European Control Conference (ECC), 2015, pp. 2216–2221.

[19] C. K. Enyioha, *A Convex Framework for Epidemic Control in Networks*, University of Pennsylvania, 2014.
[20] A. Fall, A. Iggidr, G. Sallet, and J.-J. Tewa, *Epidemiological models and lyapunov functions*, Math. Model. Nat. Phenom., 2 (2007), pp. 62–83.
[21] L. Ferretti, C. Wymant, M. Kendall, L. Zhao, A. Nurtay, L. Abeler-Dörner, M. Parker, D. Bonsall, and C. Fraser, *Quantifying SARS-CoV-2 transmission suggests epidemic control with digital contact tracing*, Science, 368 (2020).
[22] Y. Ghaedsharaf, M. Siami, C. Somarakis, and N. Motee, *Eminence in presence of time-delay and structured uncertainties in linear consensus networks*, in Proceedings of the 2017 IEEE 56th Annual Conference on Decision and Control (CDC), IEEE, 2017, pp. 3218–3223.
[23] Y. Ghaedsharaf, M. Siami, C. Somarakis, and N. Motee, *Performance improvement in noisy linear consensus networks with time-delay*, IEEE Trans. Automat. Control, 64 (2018), pp. 2457–2472.
[24] C. Godsil and J. Smith, *Strongly Cospectral Vertices*, preprint, arXiv:1709.07975, 2017.
[25] S. Hod, *Analytic treatment of the network synchronization problem with time delays*, Phys. Rev. Lett., 105 (2010), 208701.
[26] D. Hunt, G. Korniss, and B. K. Szymanski, *Network synchronization in a noisy environment with time delays: Fundamental limits and trade-offs*, Phys. Rev. Lett., 105 (2010), 068701.
[27] E. Jarlebring, J. Vanbiervliet, and W. Michiels, *Characterizing and computing the H2 norm of time-delay systems by solving the delay Lyapunov equation*, IEEE Trans. Automat. Control, 4 (2011), pp. 814–825.
[28] A. Kaddar, A. Abta, and H. T. Alaoui, *A comparison of delayed SIR and SEIR epidemic models*, Nonlinear Anal. Model. Control, 16 (2011), pp. 181–190.
[29] L. Katz, *A new status index derived from sociometric analysis*, Psychometrika, 18 (1953), pp. 39–43.
[30] E. Kaxiras and G. Neofotistos, *Multiple epidemic wave model of the COVID-19 pandemic: Modeling study*, J. Med. Internet Res., 22 (2020), e20912.
[31] D. H. Knipl, G. Röst, and J. Wu, *Epidemic spread and variation of peak times in connected regions due to travel-related infections—dynamics of an antigravity-type delay differential model*, SIAM J. Appl. Dyn. Syst., 12 (2013), pp. 1722–1762, https://doi.org/10.1137/130914127.
[32] A. L. Krause, L. Kurowski, K. Yawar, and R. A. Van Gorder, *Stochastic epidemic metapopulation models on networks: SIS dynamics and control strategies*, J. Theor. Biol., 449 (2018), pp. 35–52.
[33] K. Li, G. Zhu, Z. Ma, and L. Chen, *Dynamic stability of an SIQS epidemic network and its optimal control*, Commun. Nonlinear Sci. Numer. Simul., 66 (2019), pp. 84–95.
[34] M. Y. Li and J. S. Muldowney, *Global stability for the SEIR model in epidemiology*, Math. Biosci., 125 (1995), pp. 155–164.
[35] M. Y. Li and Z. Shuai, *Global stability of an epidemic model in a patchy environment*, Canad. Appl. Math. Quart., 17 (2009), pp. 175–187.
[36] A. L. Lloyd and V. A. Jansen, *Spatiotemporal dynamics of epidemics: Synchrony in metapopulation models*, Math. Biosci., (2004), pp. 1–16.
[37] M. Liu, X. Fu, J. Zhang, and D. Zhao, *Global dynamics of an SIS model on metapopulation networks with demographics*, Complexity, 2021 (2021), 8884236.
[38] P.-L. Liu and T.-J. Su, *Robust stability of interval time-delay systems with delay-dependence*, Syst. Control Lett., 33 (1998), pp. 231–239.
[39] S. A. Moon, F. D. Sahneh, and C. Scoglio, *Generalized Group-based Epidemic Model for Spreading Processes on Networks: GgroupEM*, preprint, arXiv:1908.06057, 2019.
[40] H. Moradian and S. S. Kia, *On the positive effect of delay on the rate of convergence of a class of linear time-delayed systems*, IEEE Trans. Automat. Control, 65 (2019), pp. 4832–4839.
[41] I. Neri and L. Gammaitoni, *Role of fluctuations in epidemic resurgence after a lockdown*, Sci. Rep., 11 (2021), pp. 1–6.
[42] I. Nesteruk, *Waves of COVID-19 Pandemic Detection and SIR Simulations*, medRxiv, 2020.
[43] C. Nowzari, V. M. Preciado, and G. J. Pappas, *Analysis and control of epidemics: A survey of spreading processes on complex networks*, IEEE Control Syst. Mag., 36 (2016), pp. 26–46.
[44] R. Olfati-Saber and R. M. Murray, *Consensus problems in networks of agents with switching topology and time-delays*, IEEE Trans. Automat. Control, 49 (2004), pp. 1520–1533.

[45] N. Olgac and R. Sipahi, *An exact method for the stability analysis of time-delayed linear time-invariant (LTI) systems*, IEEE Trans. Automat. Control, 47 (2002), pp. 793–797, https://doi.org/10.1109/TAC.2002.1000275.
[46] T. Opsahl, *The Network of Airports in the United States*, 2010, https://toreopsahl.com/datasets/#usairports (accessed October 26, 2020).
[47] C. W. Potter, *A history of influenza*, J. Appl. Microbiol., 91 (2001), pp. 572–579.
[48] V. Preciado, M. Zargham, C. Enyioha, A. Jadbabaie, and G. J. Pappas, *Optimal resource allocation for network protection against spreading processes,* IEEE Trans. Control Netw. Syst., (2014), pp. 99–108.
[49] V. M. Preciado and A. Jadbabaie, *Spectral analysis of virus spreading in random geometric networks*, in Proceedings of the 48th IEEE Conference on Decision and Control (CDC) held jointly with 2009 28th Chinese Control Conference, IEEE, 2009, pp. 4802–4807.
[50] V. M. Preciado and M. Zargham, *Traffic optimization to control epidemic outbreaks in metapopulation models*, in Proceedings of the 2013 IEEE Global Conference on Signal and Information Processing, IEEE, 2013, pp. 847–850.
[51] V. M. Preciado, M. Zargham, C. Enyioha, A. Jadbabaie, and G. Pappas, *Optimal vaccine allocation to control epidemic outbreaks in arbitrary networks*, in Proceedings of the 52nd IEEE Conference on Decision and Control, IEEE, 2013, pp. 7486–7491.
[52] W. Qiao and R. Sipahi, *A linear time-invariant consensus dynamics with homogeneous delays: Analytical study and synthesis of rightmost eigenvalues*, SIAM J. Control Optim., 51 (2013), pp. 3971–3992, https://doi.org/10.1137/110832574.
[53] W. Qiu, S. Rutherford, A. Mao, and C. Chu, *The pandemic and its impacts*, Health Culture Soc., 9 (2017), pp. 1–11.
[54] Z. Rekasius, *A stability test for systems with delays*, in Proceedings of the Joint Automatic Control Conference, Vol. 17, IEEE, 1980, p. 39.
[55] T. Sarkar, M. Roozbehani, and M. A. Dahleh, *Asymptotic network robustness*, IEEE Trans. Control Network Syst., 6 (2018), pp. 812–821.
[56] K. Savla, J. S. Shamma, and M. A. Dahleh, *Network effects on the robustness of dynamic systems*, Annu. Rev. Control Robot. Auton. Syst., 3 (2020), pp. 115–149.
[57] F. Sélley, Á Besenyei, I. Z. Kiss, and P. L. Simon, *Dynamic control of modern, network-based epidemic models*, SIAM J. Appl. Dyn. Syst., 14 (2015), pp. 168–187, https://doi.org/10.1137/130947039.
[58] Z. Shuai and P. van den Driessche, *Global stability of infectious disease models using Lyapunov functions*, SIAM J. Appl. Math., 73 (2013), pp. 1513–1532, https://doi.org/10.1137/120876642.
[59] M. Siami, S. Bolouki, B. Bamieh, and N. Motee, *Centrality measures in linear consensus networks with structured network uncertainties*, IEEE Trans. Control Netw. Syst., 5 (2017), pp. 924–934.
[60] M. Siami and N. Motee, *Fundamental limits and tradeoffs on disturbance propagation in linear dynamical networks*, IEEE Trans. Automat. Control, 61 (2016), pp. 4055–4062.
[61] B. Tang, W. Zhou, X. Wang, H. Wu, Y. Xiao, and S. Tang, *Controlling Multiple COVID-19 Epidemic Waves: An Insight from a Multi-scale Model Linking the Behavior Change Dynamics to the Disease Transmission Dynamics*, medRxiv, 2021.
[62] A. J. Terry, *Pulse vaccination strategies in a metapopulation SIR model*, Math. Biosci. Eng., 7 (2010), pp. 455–477.
[63] L. Torres, K. S. Chan, H. Tong, and T. Eliassi-Rad, *Nonbacktracking eigenvalues under node removal: X-centrality and targeted immunization*, SIAM J. Math. Data Sci., 3 (2021), pp. 656–675, https://doi.org/10.1137/20M1352132.
[64] T. W. Valente, K. Coronges, C. Lakon, and E. Costenbader, *How correlated are network centrality measures?*, Connect (Tor.), 28 (2008), pp. 16–26.
[65] P. Van Mieghem, *The N-intertwined SIS epidemic network model*, Computing, 93 (2011), pp. 147–169.
[66] P. Van Mieghem, J. Omic, and R. Kooij, *Virus spread in networks*, IEEE/ACM Trans. Netw., 17 (2008), pp. 1–14.
[67] P. Van Mieghem, D. Stevanović, F. Kuipers, C. Li, R. Van De Bovenkamp, D. Liu, and H. Wang, *Decreasing the spectral radius of a graph by link removals*, Phys. Rev. E, 84 (2011), 016101.

[68] P. Van Mieghem and R. van de Bovenkamp, *Accuracy criterion for the mean-field approximation in susceptible-infected-susceptible epidemics on networks*, Phys. Rev. E, 91 (2015), 032812.
[69] H. Wan and Jing′an Cui, *An SEIS epidemic model with transport-related infection*, J. Theor. Biol., 247 (2007), pp. 507–524.
[70] S. Xu and J. Lam, *Improved delay-dependent stability criteria for time-delay systems*, IEEE Trans. Automat. Control, 50 (2005), pp. 384–387.
[71] Z. Xu and D. Z. Sui, *Effect of small-world networks on epidemic propagation and intervention*, Geogr. Anal., 41 (2009), pp. 263–282.
[72] P. Yan and S. Liu, *SEIR epidemic model with delay*, ANZIAM J., 48 (2006), pp. 119–134.
[73] G. F. Young, L. Scardovi, and N. E. Leonard, *Robustness of noisy consensus dynamics with directed communication*, in Proceedings of the American Control Conference (ACC), 2010, IEEE, 2010, pp. 6312–6317.
[74] D. H. Zanette and M. Kuperman, *Effects of immunization in small-world epidemics*, Phys. A, 309 (2002), pp. 445–452.
[75] G. S. Zaric and M. L. Brandeau, *Resource allocation for epidemic control over short time horizons*, Math. Biosci., 171 (2001), pp. 33–58.
[76] G. S. Zaric and M. L. Brandeau, *Dynamic resource allocation for epidemic control in multiple populations*, Math. Med. Biol., 19 (2002), pp. 235–255.
[77] S. Zou, J. Wu, and Y. Chen, *Multiple epidemic waves in delayed susceptible-infected-recovered models on complex networks*, Phys. Rev. E, 83 (2011), 056121.